SCIENCE CHINA
Earth Sciences

• RESEARCH PAPER •

June 2014 Vol.57 No.6: 1325–1339
doi: 10.1007/s11430-013-4785-0

A soil water and heat transfer model including changes in soil frost and thaw fronts

WANG AiWen[1,2,4], XIE ZhengHui[1*], FENG XiaoBing[3], TIAN XiangJun[1] & QIN PeiHua[1]

[1] *LASG, Institute of Atmospheric Physics, Chinese Academy of Sciences, Beijing 100029, China;*
[2] *School of Applied Science, Beijing Information and Science Technology University, Beijing 100192, China;*
[3] *Department of Mathematics, University of Tennessee, Knoxville TN 37996, USA;*
[4] *University of Chinese Academy of Sciences, Beijing 100049, China*

Received February 10, 2013; accepted August 1, 2013; published online January 26, 2014

Freeze-thaw processes in soils, including changes in frost and thaw fronts (FTFs), are important physical processes. The movement of FTFs affects soil hydrothermal characteristics, as well as energy and water exchanges between the land surface and the atmosphere and hydrothermal processes in the land surface. This paper reduces the issue of soil freezing and thawing to a multiple moving-boundary problem and develops a soil water and heat transfer model which considers the effects of FTF on soil hydrothermal processes. A local adaptive variable-grid method is used to discretize the model. Sensitivity tests based on the hierarchical structure of the Community Land Model (CLM) show that multiple FTFs can be continuously tracked, which overcomes the difficulties of isotherms that cannot simultaneously simulate multiple FTFs in the same soil layer. The local adaptive variable-grid method is stable and offers computational efficiency several times greater than the high-resolution case. The simulated FTF depths, soil temperatures, and soil moisture values fit well with the observed data, which further demonstrates the potential application of this simulation to the land-surface process model.

soil frost and thaw fronts, soil water and heat transfer model, moving-boundary problems

Citation: Wang A W, Xie Z H, Feng X B, et al. 2014. A soil water and heat transfer model including changes in soil frost and thaw fronts. Science China: Earth Sciences, 57: 1325−1339, doi: 10.1007/s11430-013-4785-0

Freeze-thaw processes in soils, including changes in the FTF, are important physical processes. The movement of FTF positions (depths) (Chubylisku et al., 1992) affects soil hydrothermal characteristics, as well as energy and water exchanges between the land surface and the atmosphere and hydrothermal processes in the land surface. In seasonally frozen areas, the maximum frost depth is considered as an important parameter to design roadbeds to prevent heaving (DeGaetano et al., 2001). In permafrost regions, deepening of the active layer will lead to land subsidence, impacting oil and gas pipelines and related facilities (Nelson et al., 2001). At the same time, organic carbon and greenhouse gases stored in the permafrost will be gradually released into the atmosphere. Studies have shown that methane emissions will increase by 38% when the thickness of the active layer increases by 10 cm in the Arctic (Zhuang et al., 2004). Therefore, the movement of soil FTF impacts the terrestrial-ecosystem carbon cycle as well as local and even global climate change (Zhang et al., 2001; Wang et al., 2003). Long-term changes in FTF depths are an important indicator of climate change (Yi et al., 2006; Frauenfeld et al., 2004). The area of frozen soil accounts for approximately 50% of the earth's land. In China, the area of frozen soil is equivalent to 75% of land surface and permafrost is distributed mainly in mountain areas in the middle and low lati-

*Corresponding author (email: zxie@lasg.iap.ac.cn)

tudes of the Qinghai-Tibet Plateau and to the northeast and west (Xu et al., 2001; Li et al., 2008). Therefore, the movement of soil FTF has important implications on soil hydrothermal processes.

Since the 1970s, research into soil freezing and thawing processes has made significant progress. Harlan (Harlan, 1973), who thought that unfrozen water migration in frozen soil was similar to moisture migration in unsaturated soil, constructed the first hydrothermal coupled-migration model. Various modifications to this model have been made on the basis of laboratory experiments under closed and evaporation conditions (Taylor et al., 1978; Fuchs et al., 1978; Flerchinger et al., 1989; Zhao et al., 1997). With the help of field observations, soil water and heat coupling models for different needs and the corresponding numerical simulation algorithms have been developed. Related studies include the following: Hu et al. (2006) established a one-dimensional vegetation-atmosphere continuum model considering soil freezing and thawing, soil moisture fluxes, vegetation cover, and water heat exchange between the land surface and the atmospheric surface layer. The water-movement equation uses the hybrid Richards equation with various boundary conditions. Sun (2005), Zhang et al. (2007), and Li et al. (2007, 2010) developed a universal water and heat transfer model that performed magnitude analysis for various terms in the mass and energy balance equations. To study the migration laws of soil under deferent vegetation cover, Ren et al. (1998) developed a two-dimensional soil water and heat coupling model based on a one-dimensional soil water and heat coupling model. According to the basic equations of soil water and heat transfer in freezing conditions, Lei et al. (1988), Li et al. (1995), and Yang et al. (1988) used a finite-difference scheme with variable size and time steps to simulate the freezing process in a horizontal or vertical soil column. Shang et al. (1997, 2009) improved the numerical simulation process described above and deduced a new set of coupled equations for frozen soil, which simplify greatly the coupled iterative solution of the model. These studies have advanced research into soil hydrothermal coupling migration; however, they fail to consider the movement of soil at the FTF and its influence on soil hydrothermal processes.

There are many ways to estimate FTF depth. A typical method is to interpolate soil temperatures (observed or simulated) to obtain a vertical temperature distribution and to calculate FTF depth. However, multiple FTFs cannot be simulated at the same time by this method when the observed layer or the modeled layer is thick. This direct method of calculating FTF depth will also produce numerical oscillations (Yi et al., 2006) when the soil temperature is close to the freezing or melting point during the autumn freezing and spring snowmelt periods. Semi-empirical methods of calculating FTF depth, which are combined parametric methods, include the Stefan method (Stefan, 1998; Kersten, 1959; Zhang et al., 1998; Li et al., 2003; Woo et al., 2004), which used surface temperature to calculate single-column FTF depths, and Nelson method (Nelson et al., 1983; Wang et al., 2009), which considered the role of snow in temperature attenuation. These methods fail to consider the heat capacity and heat-transfer rate of the soil, and the calculated error of soil FTF depths increases with decreasing soil moisture content (Zhang et al., 2001; Woo et al., 2004; Pang et al., 2006). Methods of calculating FTF depths using a mathematical model based on physical principles focus on energy-change process in the soil. Soil moisture content under freeze-thaw conditions determines the solid-to-liquid ratio and thereby affects soil hydrothermal features (Hansson et al., 2004). Therefore, the coupling of changes in FTF with soil water and heat must be considered. In recent years, a number of land-surface models describing permafrost hydrothermal processes have been developed, such as BATS (Dickinson et al., 1993), SSIB (Xue et al., 1996), SIB2 (Sellers et al., 1996), VIC (Cherkauer et al., 1999), SHAW (Flerchinger, 2000), CoupModel (Jansson et al., 2001), COLM (Dai et al., 2007), and CLM (Oleson et al., 2010). Their soil freezing and thawing process parameters describe FTF depth as a diagnostic variable. The thick soil stratification and the uniformity of hydrothermal properties in each layer may cause the simulated freezing and melting process to run faster or slower than the real process (Li et al., 2002). To parametrize frozen soil, the soil FTF depths are needed as predictive variables to describe accurately the effects of FTF movement on land-surface hydrothermal processes. Recent work (Xie et al., 2008) in a hierarchical high-resolution structure explicitly tracks dynamic changes in FTF depth by calculating the moving interface between the freezing zone and the unfrozen zone.

This research has reduced the issue of soil freezing and thawing to a multiple moving-boundary problem considering unfrozen water and has developed a soil water and heat transfer model, which considers the effect of FTF depth on water and heat processes. A local adaptive variable-grid method has been used to discretize the model based on the hierarchical structure of the Community Land Model (CLM).

1 A soil water and heat transfer model including changes in soil frost and thaw fronts

1.1 A soil water and heat coupling moving-boundary problem including changes in soil frost and thaw fronts

Let us consider freezing and thawing problems for a one-dimensional vertical soil column. Let $(0, L)$ be a one-dimensional vertical soil column, where $z=0$ is the surface and $z=L$ is the bottom of the soil column. Assume that the soil is rigid and that soil deformation does not occur in the freeze-thaw process; that groundwater recharge and soil frost heave will not be considered; that the process of moisture migration does not include solute transport; that the position of the T_f °C isotherm (where the soil starts to freeze or thaw) is

defined as the soil FTF position; and that the soil column is divided into soil-water zones and soil-ice-water mixed zones by the phase-change interface (Figure 1).

1.1.1 Governing equations

Based on mass and energy conservation equations and continuity of soil temperature and soil volumetric water content on the phase-change interfaces, the soil freezing and thawing process equations can be written as follows (Shang et al., 1997, 2009):

$$\begin{cases} \dfrac{\partial\left(C(z,t)T\right)}{\partial t}=\dfrac{\partial}{\partial}\left(\lambda(z,t)\dfrac{\partial T}{\partial z}\right), \\ \dfrac{\partial\theta}{\partial t}=\dfrac{\partial}{\partial z}\left(D(\theta)\dfrac{\partial\theta}{\partial z}\right)-\dfrac{\partial K(\theta)}{\partial z}, \end{cases} z\in R_{\mathrm{j}},\ R_{\mathrm{j}}\text{ is soil water zone,} \tag{1}$$

$$\begin{cases} \dfrac{\partial\left(Ce(z,t)T\right)}{\partial t}=\dfrac{\partial}{\partial z}\left(\lambda e(z,t)\dfrac{\partial T}{\partial z}\right)-Ue\dfrac{\partial T}{\partial z}, \\ \dfrac{\partial\theta}{\partial t}=\dfrac{\partial}{\partial z}\left(D(\theta)\dfrac{\partial\theta}{\partial z}\right)-\dfrac{\partial K(\theta)}{\partial z}-\dfrac{\rho_{\mathrm{i}}}{\rho_{\mathrm{w}}}\dfrac{\partial\theta_{\mathrm{i}}}{\partial t}, \end{cases} z\in R_{\mathrm{j}},\ R_{\mathrm{j}}\text{ is soil ice-water mixed zone.} \tag{2}$$

where t is the time (s) and z is the space (m) coordinate (positive downward); $T(z,t)$, $\theta(z,t)$, and $\theta_{\mathrm{i}}(z,t)$ represent soil temperature (K), soil unfrozen water content, and volumetric ice content at the point and at time t; ρ_{i}, ρ_{w} are the densities (kg/m^3) of ice and water; $s_j(t)$ is the j-th position of the FTF at time t; $C(z,t)$, $\lambda(z,t)$ denote the soil heat capacity and soil thermal conductivity at point z and time t; $Ce(z,t)$, $\lambda e(z,t)$, and $Ue(z,t)$ are the equivalent volumetric heat capacity, the equivalent thermal conductivity, and the equivalent convection velocity; $D(\theta)$ (m^2 s^{-1}) and $K(\theta)$ (m^2 s^{-1}) are the unsaturated soil hydraulic diffusivity and the unsaturated soil hydraulic conductivity for the equations of soil hydrothermal parameters, see Appendix 1 (link.springer.com).

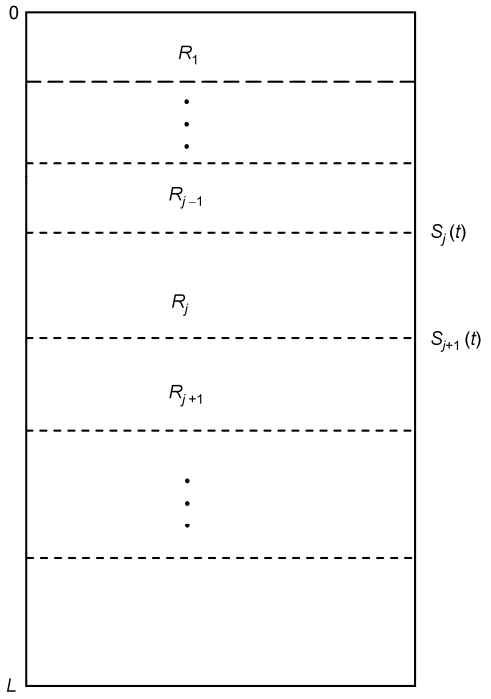

Figure 1 Schematic diagram of soil freezing and thawing.

There are three unknown quantities in eq. (2): the soil unfrozen water content θ, the volumetric ice content θ_{i}, and the soil temperature T, and therefore another relation is needed. This relationship (Niu et al., 2006) is based on two theories: one relates soil-water potential and temperature, and the other uses the inherent soil hydraulic-properties constitutive relations to determine the relationship between soil moisture and temperature:

$$\theta_{\max}=\theta_{\mathrm{s}}\left[\frac{L_{\mathrm{i}}(T-T_{\mathrm{f}})}{g\psi_{\mathrm{s}}T_{\mathrm{f}}}\right]^{\frac{1}{b}},\ T<T_{\mathrm{f}}\ , \tag{3}$$

Eq. (3) gives maximum unfrozen water content under soil negative temperature conditions, where g is the gravitational acceleration. Therefore, when soil is frozen, the excess unfrozen soil-water content is the soil volumetric ice content:

$$\theta_{\mathrm{i}}=\max\left(\rho_{\mathrm{w}}(\theta-\theta_{\max})/\rho_{\mathrm{i}},0\right).$$

1.1.2 Frost and thaw front equations and kinematic boundary conditions

The frost and thaw front equations are:

$$\pm Q(t)\frac{\mathrm{d}s_j(t)}{\mathrm{d}t}=\lambda(z,t)\frac{\partial T}{\partial z}\bigg|_{z=s_j(t)^+}-\lambda(z,t)\frac{\partial T}{\partial z}\bigg|_{z=s_j(t)^-}, \tag{4}$$

where $Q(t)=L_{\mathrm{i}}\rho_{\mathrm{d}}(W-W_{\mathrm{u}})$ is the phase-change heat (kJ m^{-3}) (Pang et al., 2006; Nan et al., 2004), L_{i} is the latent heat of freezing or melting of water (334.5 kJ/kg), ρ_{d} is the soil dry bulk density (kg/m^3), W is the soil water content on the interface, and W_{u} is the soil unfrozen water content at the initial freezing temperature. Eq. (4) describes the energy balance of the phase-change interface. If the j-th layer is a soil-water zone, Q is preceded by "+"; if the j-th layer is a soil-icewater mixed zone, Q is preceded by "–".

The kinematic boundary condition can be described as:

$$T(z,t)\Big|_{z=s_j^+}=T(z,t)\Big|_{z=s_j^-}=T_{\mathrm{f}}\ , \tag{5}$$

$$\left(\theta(z,t)+\frac{\rho_{\mathrm{i}}\theta_{\mathrm{i}}(z,t)}{\rho_{\mathrm{w}}}\right)\Bigg|_{z=s_j(t)^+}=\left(\theta(z,t)+\frac{\rho_{\mathrm{i}}\theta_{\mathrm{i}}(z,t)}{\rho_{\mathrm{w}}}\right)\Bigg|_{z=s_j(t)^-}. \tag{6}$$

Eqs. (5) and (6) describe the continuity of soil temperature and soil moisture respectively. Eqs. (1)–(6) and the appropriate initial and boundary conditions constitute a soil water and heat coupling moving-boundary problem including changes in soil FTF depth and are collectively denoted as Model I. This model represents the general state of the soil

column and can reflect the various states of the soil column with changes in FTF depth.

1.2 Numerical algorithms for the soil water and heat coupling model

For a numerical discretization of the soil water and heat coupling model, see Appendix 1. Assuming that the soil temperature, unfrozen water content, and FTF depth are given at time t_k, the values of all variables at $t_k+\Delta t$ can be computed as follows:

(1) Assume that the temperature of the soil layers, the unfrozen water content, and the volume ice content at time t_k are $T_{k,j}$, $\theta_{k,j}$, and $(\theta_i)_{k,j}$ (j=1, ..., J). $k1$ values of frost depth and $k2$ values of thaw depth are denoted as ξ_k^{m1}, ζ_k^{m2} ($m1$=1, ... $k1$; $m2$=1, ..., $k2$). The problem is to evaluate the position of ξ_k^{m1}, ζ_k^{m2} in soil stratification Γ_h. If $|\xi_k^{m1}-z_i|>0.02$ and $|\xi_k^{m1}-z_{i+1}|>0.02$ or $|\zeta_k^{m2}-z_i|>0.02$ and $|\zeta_k^{m2}-z_{i+1}|>0.02$, new nodes are added at the interface. The initial FTF depths are interpolated approximately using the initial temperature.

(2) If the number of nodes has been increased, assume that frost and thaw fronts coexist. First, insert frost fronts into the original layered soil structure to form a new temporary soil hierarchy Γ_{h1} with total number of nodes J_{kh1}. Update the soil temperature of each node, the unfrozen water content, and the volumetric ice content to $\overline{T}_{k,j}, \overline{\theta}_{k,j}, \left(\overline{\theta_i}\right)_{k,j}$ (j=1, ..., J_{kh1}). Then insert thaw fronts into the layered soil structure Γ_{h1} to form a new soil hierarchy $\Gamma_{h2}=\{zm_j, j=1, ..., J_k\}$, update the soil interface and the thickness of each layer, and update the soil temperature of each node, the unfrozen water content, and the volumetric ice content to $(T')_{k,j}$, $(\theta')_{k,j}$, $(\theta_i')_{k,j}$ (j=1, ..., J_k). The temperature at FTF is T_f. Unfrozen soil water content at the interface is obtained by interpolation. Then determine the soil parameters by solving eqs. (A15) and (A19), using nonlinear iteration for eq. (A19). Thus $(T')_{k+1,j}$, $(\theta')_{k+1,j}$, (j=1, ..., J_k) are obtained.

(3) According to the corresponding relationship of zm_j (j=1, ..., J_k) and z_j (j=1, ..., J), return to the original soil stratification using $(T')_{k+1,j}$, $(\theta')_{k+1,j}$ (j=1, ..., J_k) and update temperature of each node, the soil unfrozen water content, and the volumetric ice content to $(T'')_{k+1,j}$, $(\theta'')_{k+1,j}$, $(\theta_i'')_{k+1,j}$ (j= 1, ..., J) and the soil parameters.

(4) Assuming W_u=0.05 (Pang et al., 2006; Nan et al., 2004; Yang et al., 2011), the predicted values of the FTF depths $\xi_{k+1}'^{m1}$, $\zeta_{k+1}'^{m2}$ ($m1$=1, ... $k1$; $m2$=1, ..., $k2$) at time $T_k+\Delta t$ are determined by eq. (A20). Then evaluate the distance between every frost front and every thaw interface. If $|\xi_{k+1}'^{m1}-\zeta_k^{m2}|<0.005$, move and merge the interfaces and update $k1$, $k2$; the new frost interfaces $s1_{k+1}^{m1}$, $m1$=1, ..., $k11$ and thaw interfaces $s2_{k+1}^{m2}$, $m2$=1, ..., $k12$ are obtained by interpolation. Then sort the numbered interfaces in descending order. If $k11>k1$, set $k1=k11$; if $k12>k2$, set $k2=k12$. Similarly, $\xi_{k+1}'^{k11}=s1_{k+1}^{k11}$, $\zeta_{k+1}'^{k12}=s2_{k+1}^{k12}$.

(5) If $\max\left|\frac{\xi_{k+1}'^{m1}-\xi_k^{m1}}{\xi_k^{m1}}\right|>\varepsilon$, $\max\left|\frac{(T'')_{k+1,j}-T_{k,j}}{T_{k,j}}\right|>\varepsilon$, $\max\left|\frac{(\theta'')_{k+1,j}-\theta_{k,j}}{\theta_{k,j}}\right|>\varepsilon$, $\max\left|\frac{\xi'^{m1}_{k+1}-\xi_k^{m1}}{\xi_k^{m1}}\right|>\varepsilon$, then $T_{k,j}=(T'')_{k+1,j}$, $\theta_{k,j}=(\theta'')_{k+1,j}$, $(\theta_i)_{k,j}=(\theta_i'')_{k+1,j}$, j=1, ..., J; $\xi_k^{m1}=\xi_{k+1}'^{m1}$, $\zeta_k^{m2}=\zeta_{k+1}'^{m2}$ ($m1$=1, …, $k1$; $m2$=1, …, $k2$). Then repeat steps (1) through (4). Otherwise, set $(T'')_{k+1,j}$, $(\theta'')_{k+1,j}$, j=1, …, J; $\xi_{k+1}'^{m1}$, $\zeta_{k+1}'^{m2}$ to $T_{k+1,j}$, $\theta_{k+1,j}$, ξ_{k+1}^{m1}, $\zeta_{k+1}'^{m2}$ ($m1$=1, ... $k1$, $m2$=1, ..., $k2$) at time $T_k+\Delta t$.

(6) repeat steps (1) through (5).

Figure 2 shows the simulation flowchart without the iteration on FTF depth.

2 Model validation

2.1 Ideal test

To test and verify the correctness, rationality, numerical algorithm stability, and superior computational efficiency of the soil hydrothermal coupled model including changes in FTF depth, the following sensitivity tests were performed. First, by using the soil stratification framework of the CLM land-surface process model and holding the soil volumetric water content constant, the case of multiple FTFs was simulated. Second, for the case of two moving FTFs, the soil hydrothermal process was simulated using different time steps. Then, for the seventh-layer soil, the results calculated by the model proposed in this paper were compared with the results of calculations that did not consider double FTFs and did not use high-resolution soil stratification. The details of this test are described as follows.

(1) Multiple FTF simulation

Assuming that the simulated soil volumetric water content is 0.3, the upper boundary condition for the energy equation can be defined as follows:

$$Tsurf(t)=\begin{cases}-5, & t<500,\\ 5, & t<543,\\ -5, & t<550,.\\ 5, & t<555,\\ -5, & t\geqslant 555.\end{cases}$$

For the lower boundary conditions, the temperature gradients were zero. The initial soil temperature was assumed to be 5°C. Based on the hierarchical structure of the Community Land Model (CLM) (soil column 3.43 m), a simulation test was performed for 650 hours with a time step of one hour. The thermal conductivity parameters of the soil were assumed to be λ_l=0.57 Wm^{-1} K^{-1}, λ_i=2.29 Wm^{-1} K^{-1}, λ_s=7.9353 Wm^{-1} K^{-1} (Jason et al., 2001), and the heat

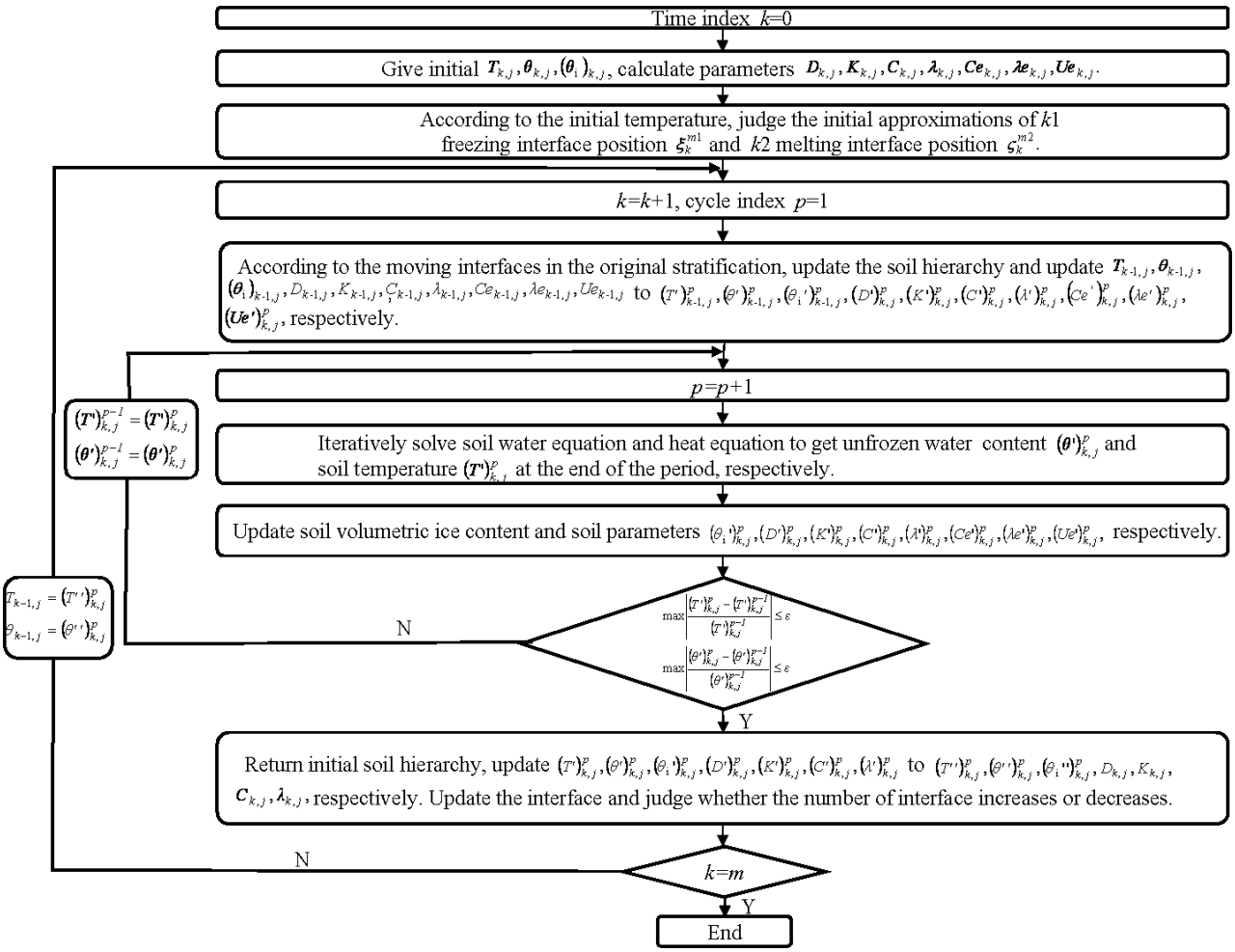

Figure 2 Simulation flow chart.

capacities were assumed to be C_w=4188 kJ m^{-3} K^{-1}, C_i=2177 kJ m^{-3} K^{-1}, C_g=2166 kJ m^{-3} K^{-1} (Jason et al., 2001). Assuming T_f=0°C, the soil temperature changed sharply after 543 h, with alternating FTFs. In Figure 3, the black areas are the soil freezing zones, and the white areas are unfrozen or melting zones. In the 550–552 hours period, four interfaces appeared simultaneously: two frost fronts and two thaw fronts (Figure 3(c)). These results show that the proposed model has the capability to continuously track multiple simulated FTFs at the same time.

(2) Comparative test

The upper boundary condition for the energy equation was given by periodic temperature boundary conditions as follows:

$$Tsurf(t)=5\cos\left(\frac{\pi t}{8760}\right).$$

Surface infiltration in the soil-water equation was zero. For the lower boundary conditions, the temperature and water flux gradients were both zero. The initial soil temperature was assumed to be 5°C, based on the hierarchical structure of the Community Land Model (CLM), and the thermodynamic parameters were the same as in test 1. Soil hydraulic parameters were set to K_s=5.23×10^{-6} m/s, ψ_s=–0.141, θ_s=0.434, b=4.74 (Li et al., 2007). A simulation test was performed for 730 days with a time step of one hour. The simulation results are shown in Figure 4.

From Figure 4(a)–4(d), it is clear that on a one-year time scale, the soil temperature, soil moisture at different soil depths, and FTF depths exhibit an obvious cyclic change with the cycle of surface temperatures. Moreover, these changes show a time lag with increasing soil depth. As shown in Figure 4(d), the top soil began to freeze from the 92nd day and the 457th day, being frozen down to 3.43 m on the 167th day and the 521st day. Then the frost depth remained at 3.43 m because the calculation of the maximum frost depth was limited to that value. From the 274th day and the 639th day, the soil began to melt, and by the 342nd day and the 710th day, the FTFs converged at 3.43 m, meaning that a freeze-thaw cycle had been completed. Figure 4(b) shows that the soil unfrozen water content suddenly decreased as the soil began to freeze and suddenly increased as the soil began to melt. Figure 4(c) shows that the soil volumetric water content gradually decreased due to its own

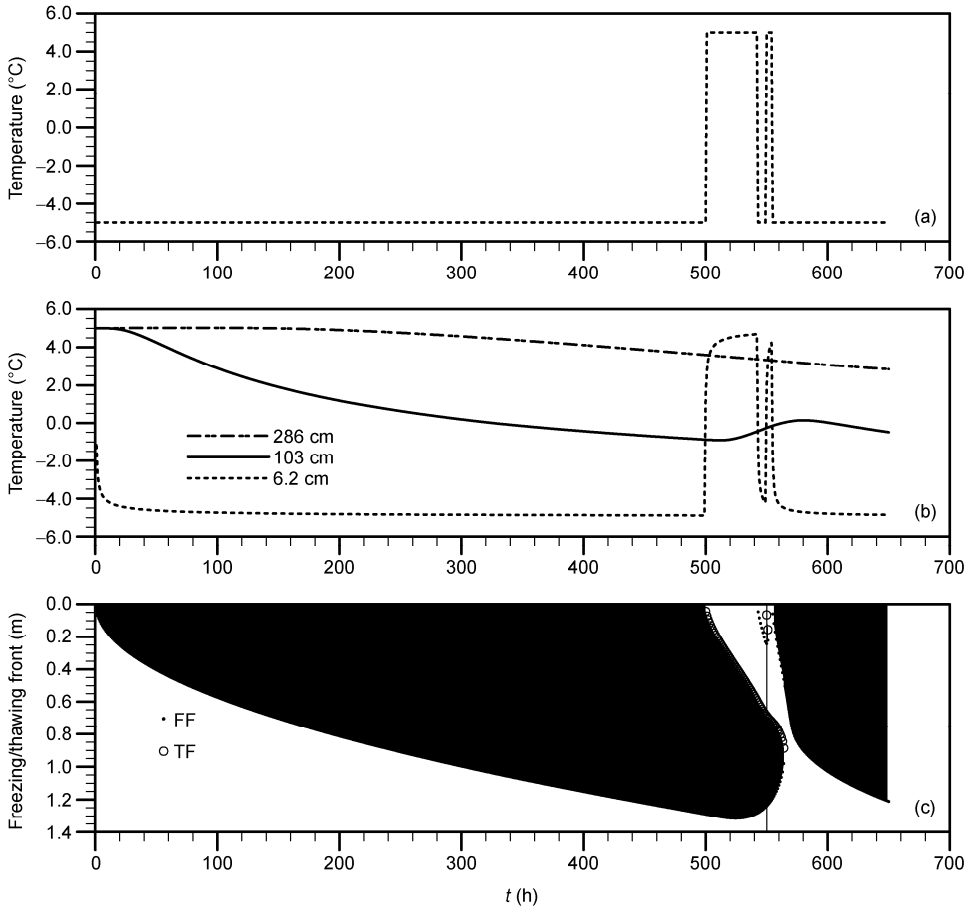

Figure 3 Soil temperature and FTF depth variations. (a) Surface temperature; (b) soil temperature; (c) FTF depth (FF: frost depth, TF: thaw depth, the black area is the frozen zone, the white area is the unfrozen zone).

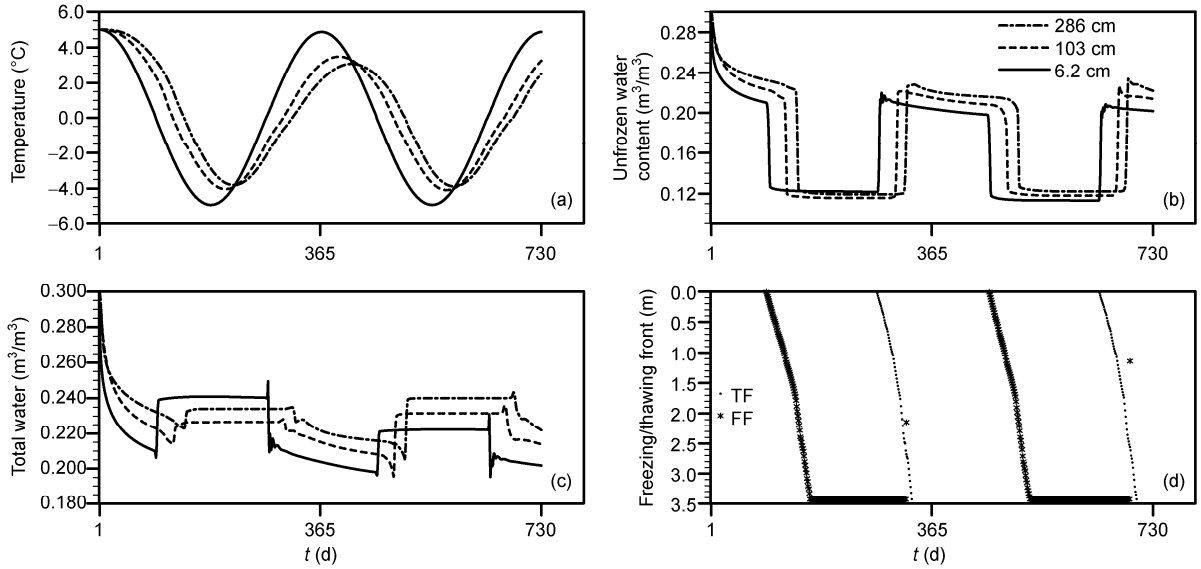

Figure 4 Soil temperature and FTF depth variation. (a) Soil temperature; (b) unfrozen soil water content; (c) total water content; (d) FTF depth (FF: frost depth, TF: thaw depth).

gravity. Upon initial freezing, a sharp decline in soil moisture occurred, and then in the early freezing phase, moisture migrated to the frozen area. This created moisture enrichment at the interface. Soil volumetric water content then quickly increased to reach a stable value. After freezing, moisture migration in the frozen zone was almost at a

standstill, and the soil moisture content of this zone remained almost unchanged because of the low unfrozen water content and ice resistance. When the soil began to melt, the moisture gathered in the upper layer moved downward, which created water enrichment at the melting interfaces, and soil volumetric water content reached a peak.

Under the experimental conditions described above, the following control tests were performed: Test 1: a double moving interface with time steps of 1800, 3600, and 7200 s. The FTF depth was obtained using the FTF equation (4). Test 2: a time step of one hour without the double moving interface. FTF depth depended on soil temperature and was determined by 0°C isotherm interpolation. Test 3: the soil column was divided into 483 parts, with each soil layer 1.75 cm thick; the time step was one hour. There was no double moving interface, and FTF depth depended on soil temperature and was determined by 0°C isotherm interpolation.

Because of hydrothermal fluctuations at the surface and varying soil depths, it is difficult to compare results. The soil hydrothermal variables in the above tests were compared for the seventh layer (49–82 cm). Figure 5 shows the calculated results for the various time steps. From Figure 5(a), 5(c), and 5(e), the simulated results for the soil variables almost coincide under the three test conditions. Using the calculated results for the 3600-second time step as a reference, the relative error of the calculated results was evaluated for the other two cases for soil temperature, soil moisture, and FTF depth. From Figure 5(b), 5(d), and 5(e), the maximum relative error of soil temperature was 0.0283, the maximum relative error of volumetric soil water content was 0.0146, and the maximum relative error of FTF depth was 0.0294. These results show that the numerical algorithm proposed in this paper is correct and stable. The simulation results from the three tests are compared in Figure 6. It is clear that the variations in simulated soil temperatures and soil volumetric water contents for the three tests are basically consistent. Due to the presence of the FTF, the soil layer structure will be more precise, and the hydrothermal parameters for thick soil layers will be more accurate. Compared with the results without the moving interface, the results of test 1 are closer to the results of test 3 during the freeze-thaw period. From Figure 6(d), the variation in FTF depth calculated from the three tests is consistent. Test 1 can continuously track the changes in interface position down to

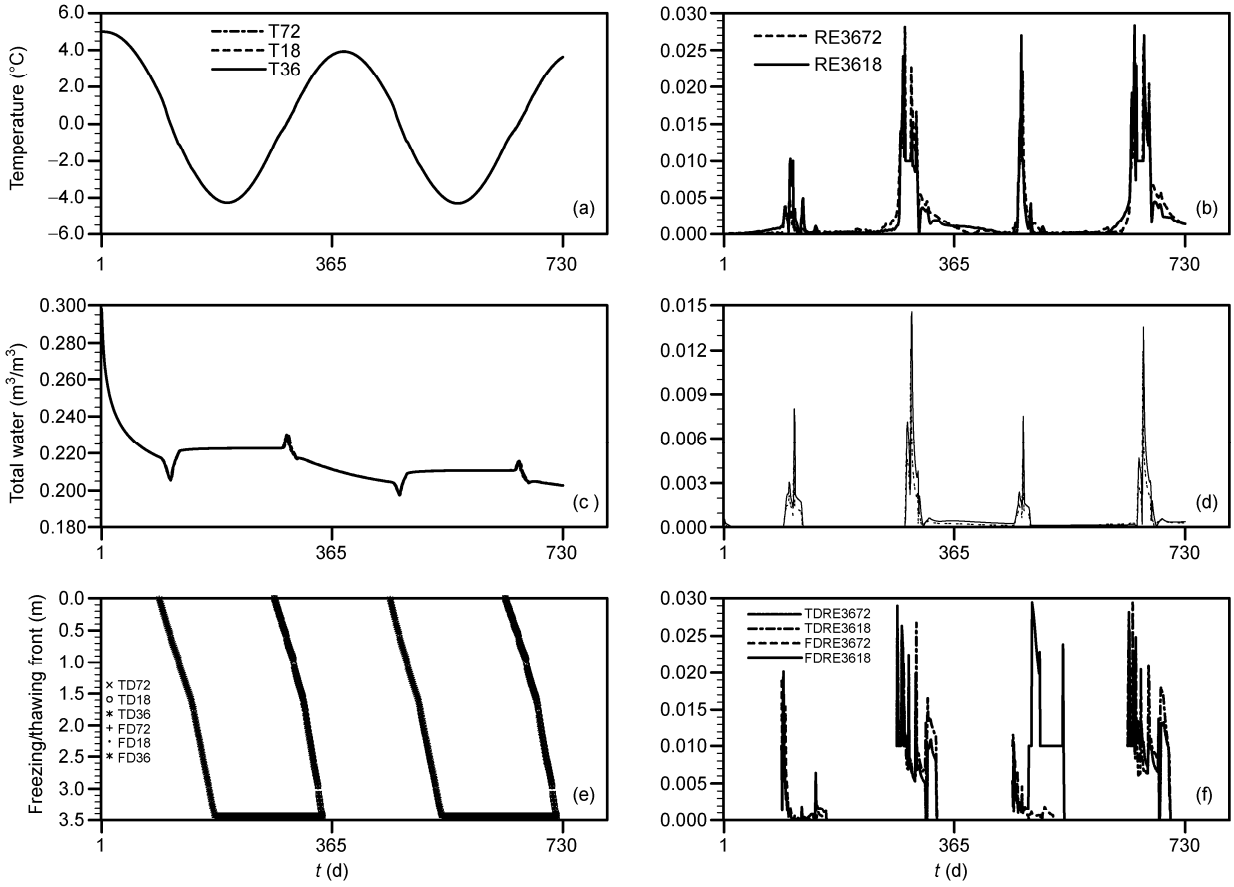

Figure 5 Comparative tests with different time steps. (a) Soil temperature; (b) soil temperature error curve (relative error among calculation results for 3600, 1800, and 7200 s time steps); (c) soil volumetric water content; (d) relative error of volumetric soil water content, calculated as for (b); (e) FTF depth; FD36, FD18, and FD72 denote the frost depth at 3600, 1800, and 7200 s time steps respectively, and TD36, TD18, and TD72 represent thaw depth at 3600, 1800, and 7200 s time steps respectively; (f) relative error of FTF depth, calculated as for (b).

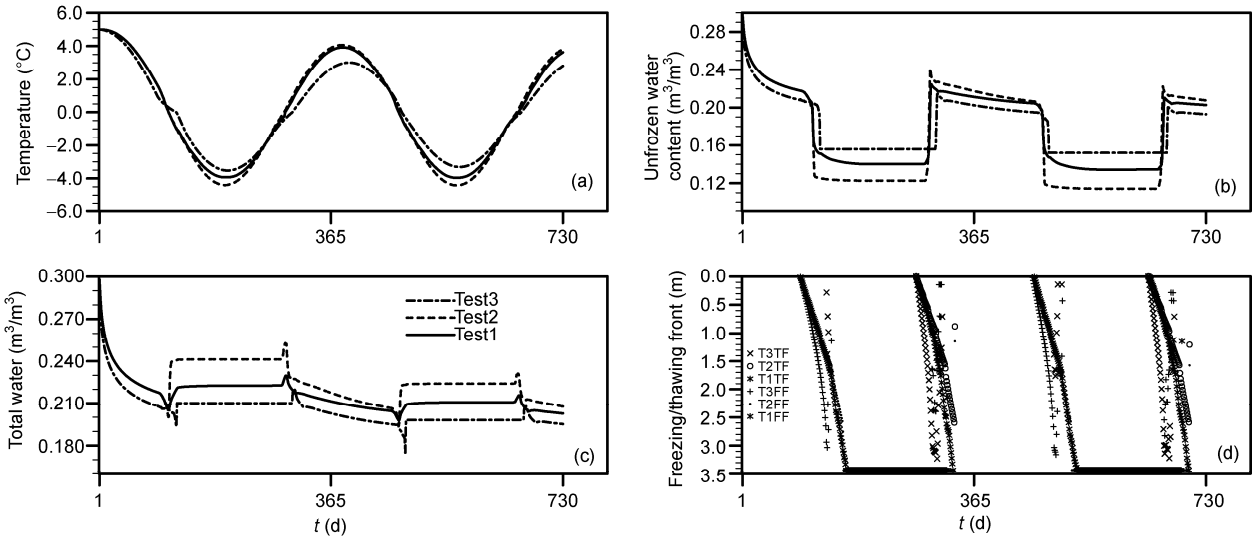

Figure 6 Soil temperature, soil moisture, and FTF depth simulated by three different algorithms for the seventh soil layer. (a) Soil temperature; (b) unfrozen soil water content; (c) soil volumetric water content; (d) FTF depth. T1FF, T2FF, and T3FF denote simulated frost depth and T1TF, T2TF, and T3TF denote simulated thaw depth in tests 1, 2, and 3.

the maximum depth of 3.43 m. The maximum FTF depth is 3.247 m as interpolated from the test 3 results, but the maximum FTF depth interpolated from the test 2 results is 2.82 m because this test was limited by the tenth-layer nodes in CLM. Because the deep soil is very thick, the FTF depths interpolated from the test 2 results were partially interrupted. As for computational efficiency, test 1 took 8.5 s and test 2 took 6 s, but test 3 took 86 s. From these results, it can be concluded that the local adaptive variable-grid algorithm proposed in this paper is reasonable, stable, and efficient.

2.2 Tibetan Plateau D66 site simulation test

D66 station (Zhang et al., 2007; Li et al., 2007; Li et al., 2010) is located in the northern part of the Tibetan Plateau (35°31′N, 93°47′E), at an altitude of 4560 m. Annual precipitation is low, the soil is non-homogeneous permafrost (Yang et al., 2000), the soil type is sandy loam with sand 58% and clay 10% (Zhang et al., 2007), and the soil starts to freeze from –0.12°C (Zhang et al., 2008). The meteorological elements of the D66 automatic weather station observations include atmospheric forcing fields of 1.5 m depth every 30 min, including incident shortwave radiation flux, air temperature, barometric pressure, relative humidity, wind speed, and surface temperature. Observations of soil temperature included surface temperature measured with an infrared radiation thermometer and 10 platinum geotemperature probes (Pt). Soil temperatures in ten layers (4, 20, 40, 60, 80, 100, 130, 160, 200, and 250 cm) were obtained from the data acquisition instrument Observations of the soil unfrozen water content included six time-domain reflectometry probes. Soil moisture values for six layers (4, 20, 60, 100, 160, and 225 cm) were obtained from the data acquisition instrument. Data for soil temperature and unfrozen water content were collected automatically once an hour.

To verify the superiority of the soil water and heat coupling model proposed in this paper, the numerical simulated results were compared with those simulated by the earlier soil water and heat coupling model (Yang et al., 1988; Shang et al., 2009) below, denoted as Model II:

$$\begin{cases} \dfrac{\partial Ce(z,t)}{\partial t} = \dfrac{\partial}{\partial z}\left(\lambda e(z,t)\dfrac{\partial T}{\partial z}\right) - Ue\dfrac{\partial T}{\partial z}, \\ \dfrac{\partial \theta}{\partial t} = \dfrac{\partial}{\partial z}\left(D(\theta)\dfrac{\partial \theta}{\partial z}\right) - \dfrac{\partial K(\theta)}{\partial t} - \dfrac{\rho_{\mathrm{i}}}{\rho_{\mathrm{w}}}\dfrac{\partial \theta_{\mathrm{i}}}{\partial t}, \end{cases} \quad 0 < z < L. \tag{7}$$

The following simulation is based on the community land-surface model (CLM) ten-layer hierarchy (the 3.43 m soil column). The observed surface soil temperature and soil infiltration flux were given as upper boundary conditions. Here the infiltration flux was obtained by driving the CLM under the NCEP forcing data and spin-up for 20 years. Zero water flux was the lower boundary condition, and the initial value was obtained by interpolation from observed variables at the starting time. The same parameters and initial and boundary conditions were used for the simulation. The simulation time span was from September 1, 1997 to September 22, 1998. The simulation was performed in three cycles under the following experimental conditions; the final results were used for analysis.

Case One: Zero heat flux was used as the lower boundary conditions for the energy equation. The calculated hydraulic characteristic parameters were the same as in ideal experiment 2. Due to severe changes in surface temperature, freeze-thaw cycles appeared repeatedly. Figure 7 shows the freeze-thaw cycle diagram simulated by model I from 0∶00

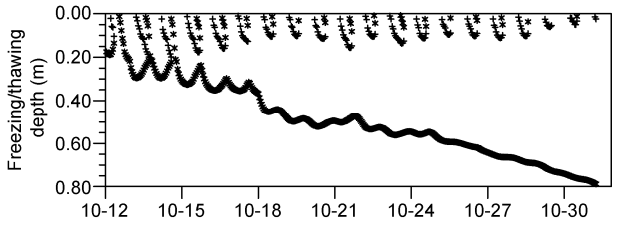

Figure 7 Freeze-thaw cycle schematic from 0:00 on October 12 to 0:00 on November 1, 1997. * indicates frost depth; + indicates thaw depth.

on October 12th to 0:00 on November 1, 1997. As can be seen from Figure 7, diurnal freeze-thaw cycles occurred within the near-surface 0.2 m. Analogously, from May 1 to June 10, 1998, two thaw fronts and a frost front often occurred. The maximum depth of the daily freeze-thaw cycle was 0.125 m. Figure 8 shows the results for soil temperature and soil unfrozen water content at 20, 60, 100, 160 cm, and the maximum FTF depth and their changes over time as simulated by Models I and II, which are also compared with observations made at the same time.

At 20 cm, for observed temperatures between 21:00 on November 6, 1997 and 4:00 on March 3, 1998, intermittent batches of data were missing. At 60 cm, between 3:00 on December 18, 1997 and 11:00 on February 11, 1998, intermittent batches of data were also missing. The trends in soil temperature and soil unfrozen water content simulated by the two models are consistent with the observations; however, during the winter freezing period, soil stratification is more refined, and the hydrothermal parameters are more accurate due to the increase in the number of computing nodes at the moving interface. Therefore, the soil temperature and soil unfrozen water content were more accurate not only during the freezing period, but also in advance of the thaw period, and the simulated trend in soil unfrozen water content was closer to the actual trend. At 20 cm, apart from a few simulation results, the difference between the values simulated by Models I and II and the observed temperatures did not exceed [–6, 4]°C. At 60 and 100 cm, the difference between the values simulated by Model I and the observed temperatures lay within [–4, 4]°C, while Model II's error range was [–5, 4]°C. At 160 cm, the difference between the values simulated by Models I and II and the observed temperatures lay within [–5, 4]°C. From Figure 8(a), 8(c), 8(e), 8(g), and 8(i), it can be seen that the interannual variability of soil-layer temperatures is consistent with surface temperature. Moreover, the change exhibits a time lag, which increases with soil depth. Figures 8(b), 8(d), 8(f), and 8(h) show that as the surface began to freeze in late October 1997, the soil unfrozen water content began to decline. As it began to thaw in April 1998, water content began to increase. The frost duration in the surface soil is up to six months or so, and the annual cycle of freeze-thaw processes is completed in mid-June. As can be seen from the simulated frost depth, the freezing process takes about two months. The frost depth reached more than 200 cm in late November, but after this, the freezing rate slowed down significantly. After three months of freezing, the soil frost depth was about 250 cm in early January. The soil continued to be frozen, but the observed maximum depth was 250 cm. Therefore, the maximum FTF depth is 250 cm in Figure 8(j). The shallow soil began to ablate in April, and the thaw continuously passed down the soil column. By July, the soil was all melted, completing an annual freeze-thaw cycle for the entire soil column. The observed depths in Figure 8(j) were determined by linearly interpolating soil temperature profiles to find the T_f °C isotherm position. The FTF depth simulated by Model II exhibits obvious numerical oscillations. For example, the T_f °C isotherm at 160 cm lasted about a month in the melt phase, then rose, which is mainly due to the interpolation assumption that an entire soil layer can be either in a frozen or a melted state; the two states cannot coexist. The depth simulation by Model I avoids this phenomenon. As can be seen from Figure 8 and Table 1, the simulated results for the upper layers are slightly better than those for the deep layers. The reason may be that large particulate matter exists in the deep soil, and the calculated layer is thick, with uniform characteristics of the hydrothermal parameters, so that the simulated results are relatively poor. For the same soil layer, the soil temperature, soil unfrozen water content, and FTF depth simulated by Model I were better than those simulated by Model II. This occurred because the presence of the moving interface makes the soil stratification refinement and the hydrothermal parameters more accurate. Therefore, the simulation results are slightly improved. What is more important is that the proposed model can continuously track the position of the FTF, overcoming numerical oscillations in the interpolation.

Case Two: Zero heat flux was used as the lower boundary condition. The saturated hydraulic conductivity K_s used in Case One was increased to 5.23×10^{-5} m/s; other water thermal characteristic parameters remained unchanged. In Figure 9, the simulated results are denoted as Model III. It is clear that the soil unfrozen water content overall was lower than the original. Accordingly, the soil temperature simulated by Model I was lower on the whole (Figure 8(b), 8(d), 8(f), 8(h)), but the simulated soil unfrozen water content was higher, which may have been caused by the effects of low soil hydraulic conductivity on the calculation process and by observation instrument error.

Case Three: The lower boundary condition of the soil heat equation used the heat flux calculated from measured monthly mean temperature profiles. The saturated hydraulic conductivity was set to $K_s=5.23\times10^{-5}$ m/s; other hydraulic characteristic parameters were the same as in Case One. Because measured ground temperature data from September 1997 to September 1998 at 3.43 m are missing, Table 2 shows the monthly average ground temperatures at 3.2 meters

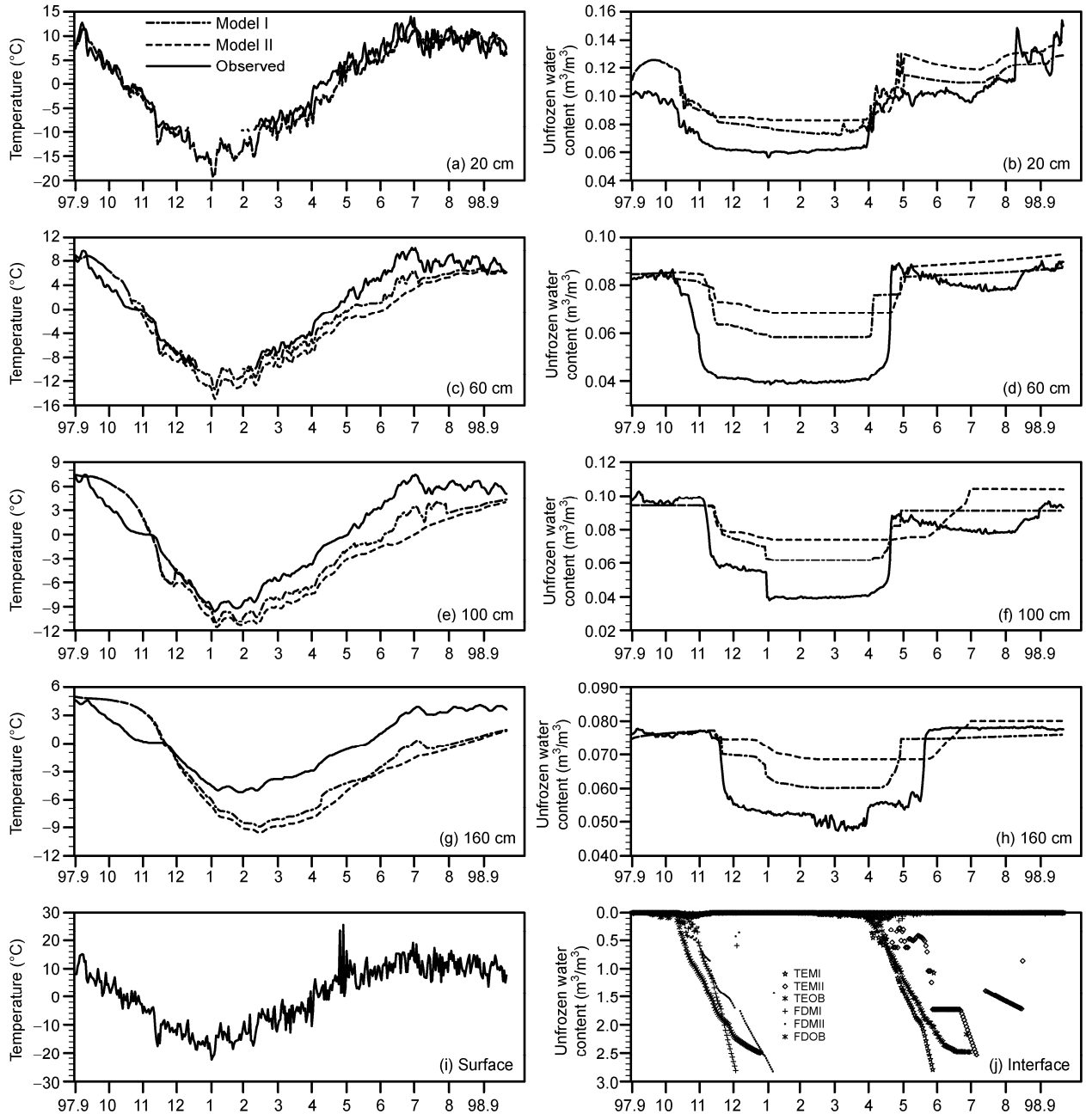

Figure 8 D66 site simulations and observations under the CLM hierarchy. Soil temperature: (a) 20 cm; (c) 60 cm; (e) 100 cm; (g) 160 cm. Unfrozen soil water content: (b) 20 cm; (d) 60 cm; (f) 100 cm; (h) 160 cm. FTF depth: (j) thaw depths simulated by Model I; TDMII: thaw depths simulated by Model II; TDOB: observed thaw depths; FDMI: frost depths simulated by Model I; FDMII: frost depths simulated by Model II; FDOB: observed frost depths; (i) surface temperatures.

and 4.0 meters from 1996 to 1997 at the D66 Daoban 2 location(Wang et al.,1999).

Using the equation $F = -\lambda \frac{\partial T}{\partial z}$, the monthly average heat flux at 3.43 m can be calculated as an hourly heat flux (see Figure 10) in the corresponding month from September 1997 to September 1998. In Figure 11, the simulated results are denoted as Model IV.

Figure 11 shows that the simulated trends of soil temperature and unfrozen water content as predicted by Models I and IV change consistently. Model IV used the heat flux calculated from the approximately measured data as a lower boundary condition. The simulated results from Model IV were slightly better than those from Model I. However, it can be seen from Figure 10 that the soil heat flux did not exceed 0.69 W/m^2 at 3.43 m at the D66 site. Therefore, the difference was slight between the lower soil results simulated by Models I and IV. It is clear from the above results

Table 1 Correlation coefficients and root mean square errors between Model I and II simulations and observations[a)]

Site	Model	Soil depth (cm)	Soil temperature		Unfrozen water content		Freeze interface maximum depth		Melt interface maximum depth	
			CC	RMSE	CC	RMSE	CC	RMSE	CC	RMSE
D66	I	20	0.96	2.20	0.92	0.02	0.71	0.53	0.78	0.69
	II	20	0.96	2.24	0.89	0.02	0.62	0.59	0.51	0.74
	I	60	0.94	2.20	0.92	0.02				
	II	60	0.91	3.27	0.90	0.02				
	I	100	0.92	2.60	0.95	0.02				
	II	100	0.88	3.60	0.71	0.02				
	I	160	0.85	3.15	0.89	0.01				
	II	160	0.82	3.75	0.81	0.01				
D110	I	20	0.99	0.62	0.96	0.04	0.75	0.43	0.78	0.63
	II	20	0.99	0.67	0.87	0.05	0.68	0.48	0.62	0.71
	I	60	0.99	1.35	0.85	0.05				
	II	60	0.98	1.76	0.81	0.07				
	I	100	0.95	2.14	0.87	0.07				
	II	100	0.94	2.50	0.85	0.08				
	I	160	0.79	2.69	0.69	0.08				
	II	160	0.77	3.16	0.61	0.08				

a) RMSE is the root mean squared error, and CC is the correlation coefficient.

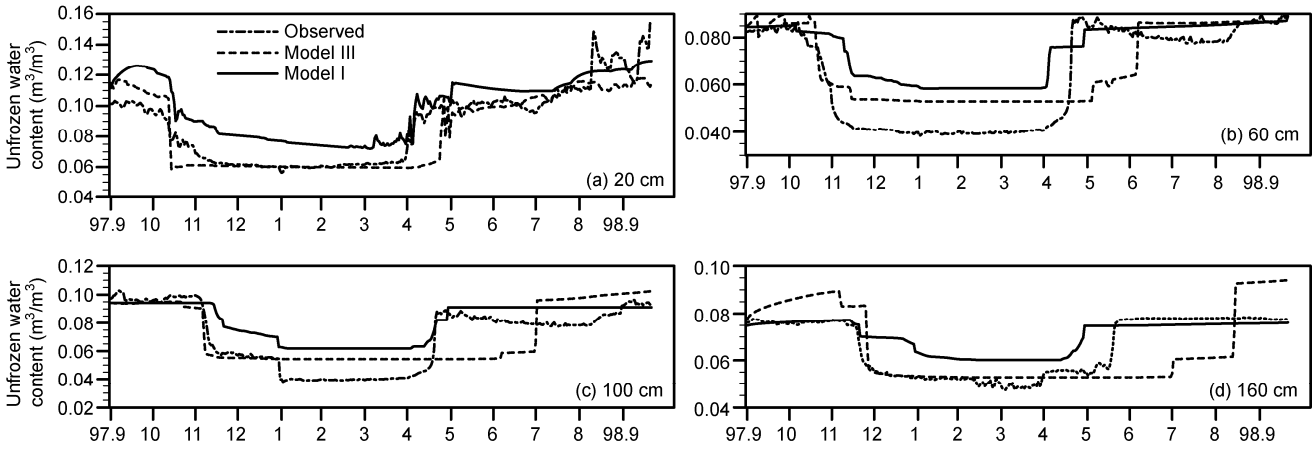

Figure 9 Observed and simulated volumetric liquid water content with different saturated hydraulic conductivity values at the D66 site. Model III: K_s=5.23×10^{-5} m/s, Model I: K_s=5.23×10^{-6} m/s.

Table 2 Monthly average ground temperature at D66 Daoban 2 location from 1996 to 1997

Time (months)	1	2	3	4	5	6	7	8	9	10	11	12
4 m	–0.49	–0.44	–0.38	–1.01	–0.80	–0.56	–0.49		–0.36	–0.37	–0.43	–0.47
3.2 m	–0.20	–0.26	–0.72	–1.24	–0.72	–0.62	–0.41	–0.05	–0.02	0.02	–0.09	–0.18

that if there are measured temperature data at the lower boundary, it is better to use the calculated heat flux as the lower boundary condition; if there are no measured ground temperature data, the variations in soil temperature and unfrozen water content can be basically simulated with zero heat flux as the lower boundary condition, as at the D66 site.

2.3 Tibetan Plateau D110 site simulation test

The D110 station (Yang et al., 1999) is located near the

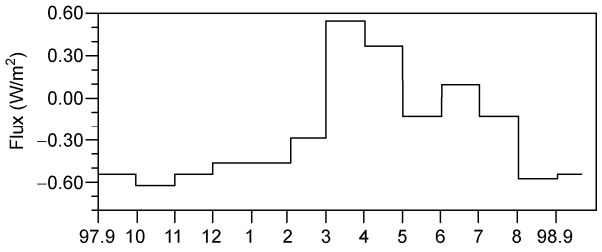

Figure 10 Schematic diagram of hourly soil heat flux at 3.43 m from 1997-09-01 to 1998-09-22 at the D66 site.

Qinghai-Tibet Highway at 110 Daoban (32°41′485″N, 92°51′267″E), on the one-level terraces on the Tsangpo south bank, at an altitude of 5000 m. The surface consists of marsh and grassy mounds with slight salinization and a vegetation cover between 30% and 40% consisting of small *Kobresia*. The soil is river sediments, with the upper part composed of coarse and fine sand, whereas the lower part is mainly fine sand with a silt lens body. The soil temperature and humidity observing system (SMTMS) was buried at different depths on August 2, 1997. The soil temperature was measured by 10 platinum ground-temperature probes (Pt) and a data acquisition instrument (DATALOG) and was recorded hourly. The burial depths of the ground temperature probes (Pt) were 0, 4, 20, 40, 60, 80, 100, 130, 160, and 180 cm. Soil moisture was measured by a time-domain reflectometer (TDR) and a data acquisition instrument, with data collected automatically and recorded hourly. The burial depths of the TDR probes were 4, 20, 60, 100, 160, and 180 cm. Here the soil moisture measured with the TDR mainly represents the unfrozen volume of water in the soil. Therefore, in the following analysis, soil moisture content refers to the soil unfrozen water content without ice.

The boundary conditions and the hydrothermal parameters

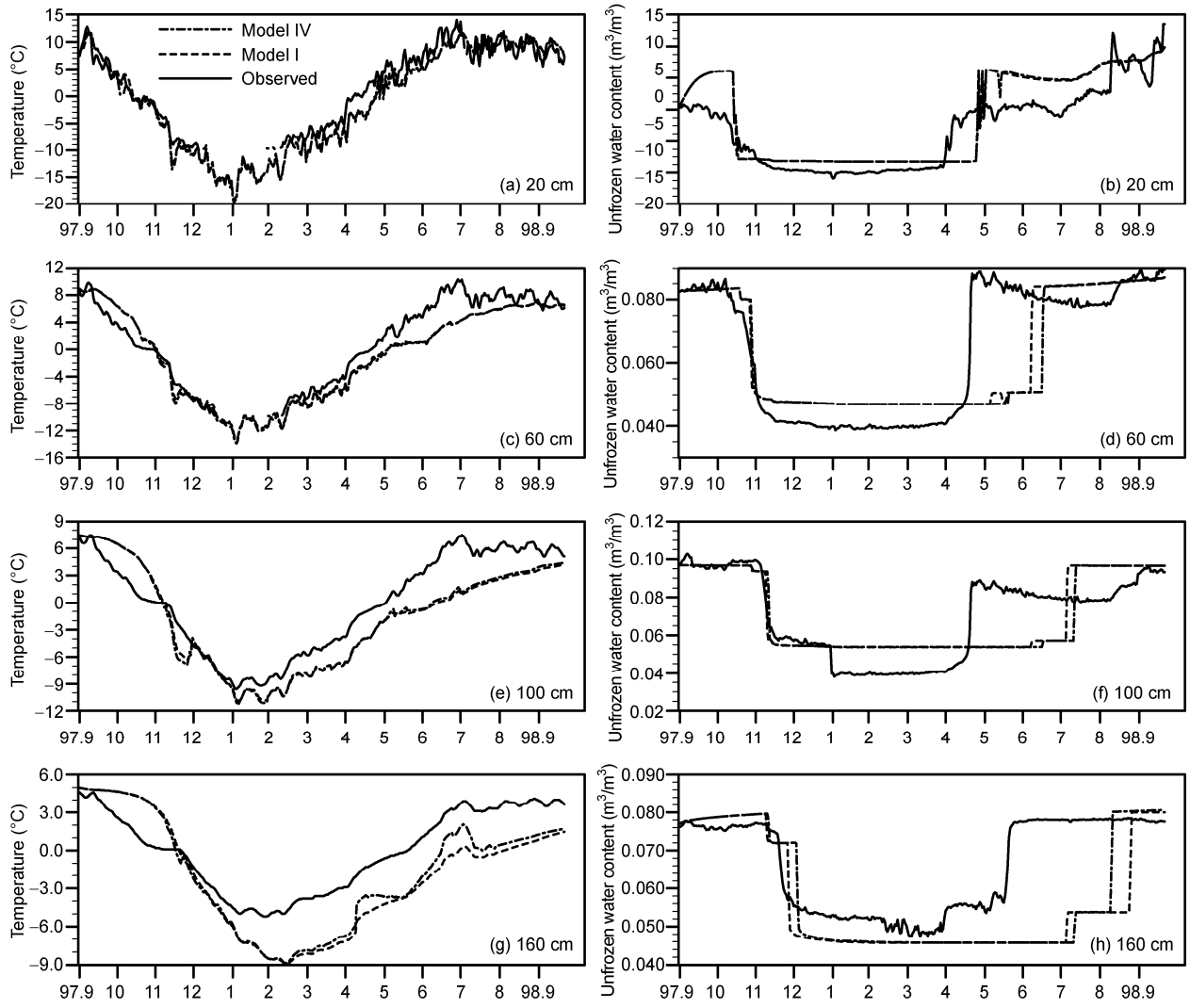

Figure 11 Simulated and observed soil temperature and unfrozen water content at the D66 site: (a), (b) 20 cm; (c), (d) 60 cm; (e), (f) 100 cm; (g), (h) 160 cm. Model IV used the heat flux calculated from the measured data as the lower boundary condition; Model I used zero heat flux as the lower boundary condition.

were the same as at the D66 site. Because there was no measured soil temperature at 3.43 m at the D110 site, zero heat flux was used as a lower boundary condition for the soil heat equation. The period from August 2, 1997 to August 31, 1998 was measured four times by an analog loop, and the final results were used for analysis. Figures 12 and 13 show the results for temperature and soil moisture as simulated respectively by Models I and II at 20, 60, 100, and 160 cm compared with observations at the same time.

At 20 cm, the difference between the simulated values from Models I and II and the observed temperatures was within [–1.5, 2]°C. At 60 cm, the difference of Model I from observed values lay within [–2.25, 2.28]°C, while Model II's error range was [–2.25, 2.62]°C. At 100 cm, the difference of Model I from observed values lay within [–2.89, 3.23]°C, while Model II's error range was [–3.29, 4.04]°C. At 160 cm, the difference between the values simulated by Models I and II and the observed temperature lay within [–5, 5]°C. From Figure 12(a), 12(b), 12(c), and 12(d), it can be seen that the interannual variability of the soil layer temperatures is consistent with the surface temperature; moreover, the change exhibits a time lag with increasing soil depth. Figure 13(a), 13(b), 13(c), and 13(d) show that as the surface began to freeze in early October 1997, the soil unfrozen water content began to decline. As the soil began to thaw in May 1998, the water content began to increase. The freezing duration of the surface soil is up to seven months, and an annual cycle of freezing and thawing processes

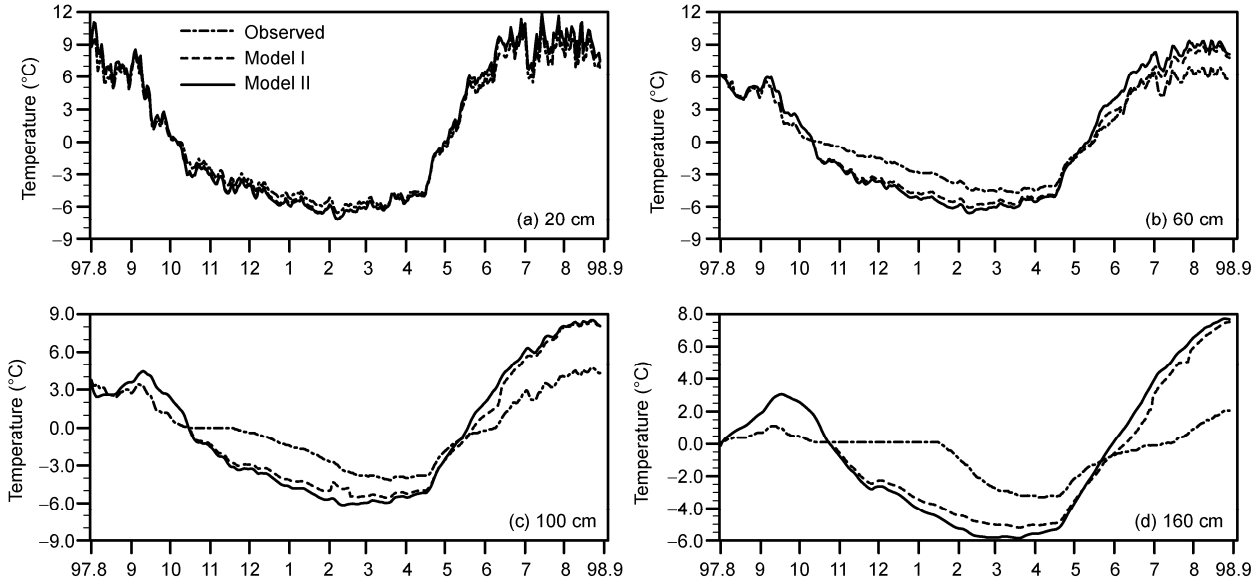

Figure 12 Simulated and observed soil temperatures at the D110 site. (a) 20 cm; (c) 60 cm; (c) 100 cm; (d) 160 cm.

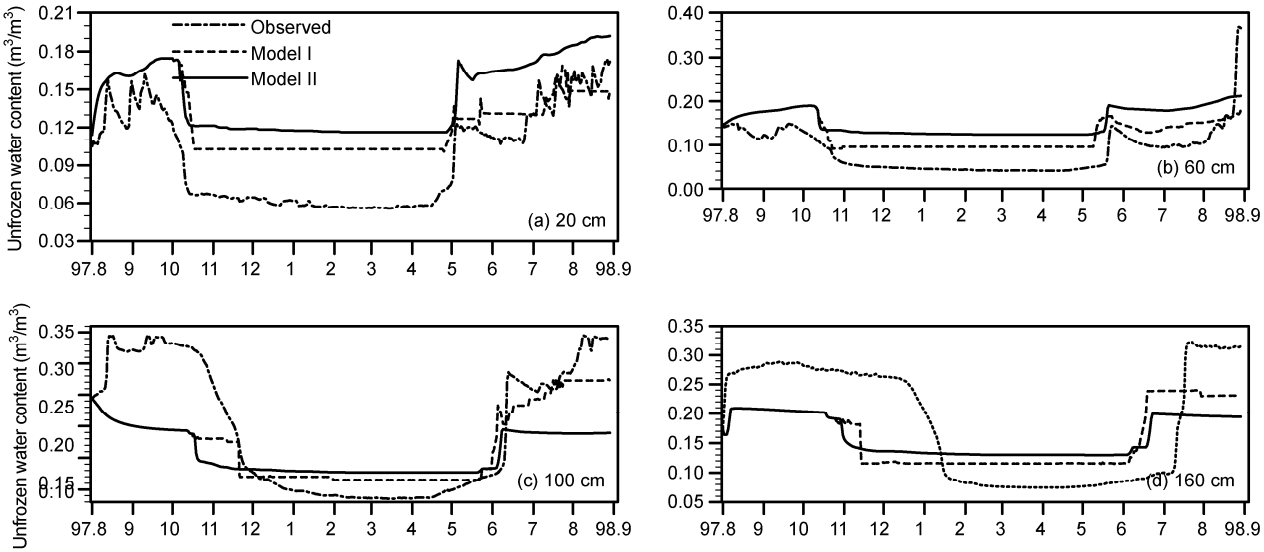

Figure 13 Simulated and observed soil unfrozen water contents at the D110 site. (a) 20 cm; (b) 60 cm; (c) 100 cm; (d) 160 cm.

is completed in late July. From Figures 12 and 13 and Table 1, it is apparent that the simulated results are similar to those at the D66 site. In the freezing period, the simulated soil temperature and soil water content were closer to reality than the predictions by Model II, and the simulated results for upper levels were better than those for deep levels. Comprehensive simulated results for the two test sites further demonstrate the potential of simulation applied to land-surface process models.

3 Discussions and conclusions

In this research, the issue of soil freezing and thawing has been reduced to a multiple moving-boundary problem. The proposed model considers FTF depth as a predictor variable which can reflect multiple states of soil freezing and thawing and can take into account the effect of FTF movement on soil hydrothermal processes. A local adaptive variable-grid method was used to discretize the model. Sensitivity tests were based on the hierarchical structure of the Community Land Model (CLM). The ability to simulate multiple FTFs and their effects on soil hydrothermal processes has been analyzed, whether or not moving interfaces are considered when the calculated structure is changed. The superiority and stability of the proposed method are apparent in the results. The simulated FTF depths, soil temperatures, and soil moisture values fit well with data observed at the D66 and D110 sites. The calculated results were much better than those obtained without considering FTF changes, which further demonstrates the reasonableness of the model as developed and the potential for application of simulation to the land-surface process model.

Although relatively good simulated results have been achieved for the two test sites studied in this research, due to the general lack of observational data (such as soil temperature, soil unfrozen water content, and FTF depth), only two permafrost sites were selected for the numerical tests. The results obtained here therefore need more validation. In addition, the underlying temperature gradient in the general land-surface model is slight, and its bottom heat-flux change is small compared with that on the surface, meaning that the heat flux for the energy equation is zero for the lower boundary condition. If there were observational data at the lower boundary, the heat flux calculated from the observed soil temperature profile could be used as the lower boundary condition. In addition, the model needs further validation and study in considering the soil T_f°C phase transition band, groundwater level changes, vegetation, snow cover, surface generalization, and a coupled land-surface process model.

This work was supported by the National Natural Science Foundation of China (Grant No. 91125016) and National Basic Research Program of China (Grants Nos. 2010CB951001, 2010CB428403). The data used in this research were obtained from the Sino-Japanese international cooperation project "Global energy and water balance experiment—Qinghai-Tibet Plateau Asian Monsoon Experiment" (GAME-Tibet), http://www.e.l.ucar.edu/pr.jects/ce.p/dm/. We thank the four anonymous reviewers for their valuable comments and suggestions, which have greatly improved the quality of the paper.

Cherkauer K A, Lettenmaier D P. 1999. Hydrologic effects of frozen soils in the upper Mississippi River Basin. J Geophys Res, 104: 19599–19610

Chubylisku B P, Kudayph B B. 1992. Determining depth of phase change front of solid water in soil (in Chinese). J Glaci Geocry, 14: 193–201

Dai Y J, Zeng X B, Dickinson R E. 2007. Common Land Model 3.5 Documentation

DeGaetano A T, Cameron M D, Wilks D S. 2001. Physical simulation of maximum seasonal soil freezing depth in the United States using routine weather observation. J Appl Meteorol, 40: 546–555

Dickinson R E, Henderson-Sellers A, Kennedy P J. 1993. Biosphere-Atmosphere Transer Scheme (BATS) version as coupled to the NCAR Community Climate Model. NCAR Tech Note

Flerchinger G N. 2000. The Simultaneous Heat and Water Model: Technical Documentation

Flerchinger G N, Saxton K E. 1989. Simultaneous heat and water model of a freezing snow-residue-soil system I: Theory and development. Trans ASABE, 32: 565–571

Frauenfeld O W, Zhang T J, Barry R G, et al. 2004. Interdecadal changes in seasonal freeze and thaw depths in Russia. J Geophys Res, 109: D05101, doi: 10.1029/2003JD004245

Fuchs M, Campbell G S, Papendick R I. 1978. An analysis of sensible and latent heat flow in a partially frozen unsaturated soil. Soil Sci Soc Amer J, 42: 379–385

Hansson K, Simunek J, Mizoguchi M, et al.2004. Water flow and heat transport in frozen soil numerical solution and freeze-thaw applications. Soil Sci Soc Am J, 3: 693–704

Harlan R L. 1973. Analysis of coupled heat-fluid transport in partially frozen soil. Water Resour Res, 9: 1314–1323

Hayashi M, Goeller N, Quinton W L, et al. 2007. A simple heat-conduction method for simulating the frost-table depth in hydrological models. Hydrol Process, 21: 2610–2622

Hu H P, Ye B S, Xu Y H, et al. 2006. A land surface model incorporated with soil freeze/thaw and its application in GAME/Tibet, China. Sci China Ser D-Earth Sci, 36: 755–766

Jansson P E, Moon D S. 2001. A coupled model of water heat and mass transfer using object orientation to improve flexibility and functionality. Environ Model Softw, 16: 37–46

Jason B, Lynch A H , Stuart C F, et al. 2001. The representation of Arctic soils in the land surface model: The importance of mosses. J Clim, 14: 3324–3335

Kersten M S. 1959. Frost penetration: Relationship to air temperature and other factors. Highw Res BoardBull, 225: 45–80

Lei Z D, Yang S X, Xie S C. 1988. Soil Water Dynamics (in Chinese). Beijing: Tsinghua University Press. 314

Li Q, Sun S F. 2007. Development of the universal and simplified soil model coupling heat and water transport. Sci China Ser D-Earth Sci, 37: 1522–1535

Li Q, Sun S F, Xue Y K. 2010. Analyses and development of a hierarchy of frozen soil models for cold region study. J Geophys Res, 115: D03107, doi: 10.1029/2009JD012530

Li S X, Cheng G D. 1995. Problems of Heat and Moisture Transfer in freezing and Thawing Soils (in Chinese). Lanzhou: Lanzhou University Press. 111–143

Li S X, Cheng G D, Guo D X. 1996. Numerical simulation of permafrost trends under the climate warming conditions. Sci China Ser D-Earth Sci, 26: 342–347

Li S X, Cheng G D. 1996. Numerical simulation of the future change of thermal regime in the high temperature permafrost of Qinghai-Tibet Plateau under climatic warming. J Glaci Geocry, 18(Suppl): 190–196

Li X, Cheng G D. 2002. Review on the interaction models between climate

system and frozen soil. J Glaci Geocry, 24: 315–321
Li X, Koike T. 2003. Frozen soil parameterization in SiB2 and its validation with GAME—Tibet observations. Cold Reg Sci Tech, 36: 165–182
Li X, Cheng G D, Jin H J, et al. 2008. Cryospheric change in China. Glob Planet Change, 62: 210–218
Nan Z T, Li S X, Cheng G D. 2004. Prediction of permafrost distribution on the Qinghai-Tibet Plateau in the next 50 and 100 years. Sci China Ser D-Earth Sci, 34: 528–534
Nelson F E, Anisimov O, Shiklomanov N. 2001. Subsidence risk from thawing permafrost. Nature, 410: 889–890
Nelson F E, Outcalt S I. 1983. A frost index number for spatial prediction of ground-frost zones. Permafrost-Fourth International Conference Proceedings. Washington DC: National Academy Press. 1: 907–911
Niu G Y, Yang Z L. 2006. Effects of frozen soil on snowmelt runoff and soil water storage at a continental scale. J Hydrometeorol, 7: 937–952
Oleson K, Lawrence D, Bonan G, et al. 2010. Technical description of version 4.0 of the Community Land Model. NCAR Tech Note
Pang Q Q, Li S C, Wu T H, et al. 2006. Simulated distribution of active layer depths in the frozen ground regions of Tibetan Plateau. J Glaci Geocry, 28: 390–395
Ren L, Zhang Y F, Shen R K. 1998. Field experiments and numerical simulation of soil water and heat regimes under the condition of strip coverage (in Chinese). J Hydraul Eng, 1: 76–85
Sellers P J, Randall D A, Collatz G J, et al. 1996. A revised land surface parameterization (SIB2) for atmosphere GCMS. Part I: Model formulation. J Clim, 9: 676–705
Shang S H, Lei Z D, Yang S X. 1997. Improvement of the numerical simulation of water and heat transfer during soil freezing (in Chinese). J Tsinghua Sci Tech, 37: 62–64
Shang S H, Mao X M, Lei Z D, et al. 2009. Soil Moisture Dynamics Simulation Model and Its Applications. Beijing: Science Press. 65–85
Stefan J. 1998. Uber die theorie der eisbildung, insbesondere yber die eisbildung im polarmeere sitzungsber akad. Wiss Wien Math Naturwiss K1 Abt, 1: 965–83
Sun S F. 2005. Physics Biochemistry and Parameterization of Land Surface Model (in Chinese). Beijing: China Meteorological Press. 53–69
Taylor G S, Luthin J N. 1978. A model for coupled heat and moisture transfer during soil freezing. Can Geotech J, 15: 548–555
Wang C H, Dong W J, Wei Z G. 2003. Study on relationship between the frozen thaw process in Qinghai Xizang Plateau and circulation in east Asia (in Chinese). Chin J Geophys, 46: 309–316
Wang C H, Jin S L, Wu Z Y. 2009. Evaluation and application of the estimation methods of frozen (thawing) depth over China. Adv Earth Sci, 24: 132–141
Wang S L, Zhao X M. 1999. Analysis of the ground temperatures monitored in permafrost regions on the Tibetan plateau (in Chinese). J Glaci Geocry, 21: 159–163
Woo M K, Arain M A, Mollinga M, et al. 2004. A two-directional freeze and thaw algorithm for hydrologic and land surface modeling. Geophys Res Lett, 31: L12501, doi: 10.1029/2004GL019475
Xie Z H, Song L Y, Feng X B. 2008. A moving boundary problem derived from heat and water transfer processes in frozen and thawed soils and its numerical simulation. Sci China Ser A-Math, 51: 1510–1521
Xu X Z, Wang J C, Zhang L X. 2001. Frozen Soil Physics. Beijing: Science Press. 10–11
Xue Y, Zeng F J, Schlosser C A. 1996. SSIB and its sensitivity to soil propertites: A case study using HAPEX-Mobility data. Global Planet Change, 13: 183–194
Yang C S, Cheng G D. 2011. Probabilistic prediction of the impacts of climate change on permafrost stability along the Qinghai-Tibet railway (II): Active layer thickness and Settlement deformation. J Glaci Geocry, 33: 469–478
Yang M X, Yao T D, Ding Y J, et al. 1999. The diurnal variation characteristics of the northern Tibetan Plateau D110 soil temperature in different seasons. Geog Sci, 19: 570–574
Yang M X, Yao T D, Gou X H. 2000. Freezing and thawing process and water-energy distribution characters along the Qinghai-Tibet road. Prog Nat Sci, 10: 443–450
Yang S X, Lei Z D, Zhu Q, et al. 1988. The numerical simulation of water and heat transfer during Soil freezing (in Chinese). J Tsinghua Sci Tech, 28: 112–120
Yi S H, Arain M A, Woo M K. 2006. Modifications of a land surface scheme for improved simulation of ground freeze-thaw in northern environments. Geophys Res Lett, 33: L13501, doi: 10.1029/2006GL026340
Zhang T, Stanmes K.1998. Impact of climatic factors on the active layer and permafrost at Barrow, Alaska. Permafrost Periglacial Process, 9: 229–246
Zhang T, Frauenfeld O W, Serreze M C, et al. 2005. Spatial and temporal variabilty in active layer thickness over the Russian Arctic drainage basin. J Geophys Res, 110: D16101, doi: 10.1029/2004JD005642
Zhang X, Sun S F, Xue Y K. 2007. Development and testing of a frozen soil parameterization for cold region studies. J Hydrmeteorol, 8: 690–701
Zhang Y S, Carey S K, Quinton W L. 2008. Evaluation of the algorithms and parameterizations for ground thawing and freezing simulation in permafrost regions. J Geophys Res, 113: D17116, doi: 10.1029/2007JD009343
Zhang Z Q, Wu Q B. 2012. Predicting changes of active layer thickness on the Qinghai-Tibet Plateau as climate warming (in Chinese). J Glaci Geocry, 34: 505–511
Zhao L T, Cray D M, Male D H. 1997. Numerical analysis of simultaneous heat and water transfer during infiltration into frozen ground. J Hydrology, 200: 345–363
Zhuang Q, Melillo J, Kicklighter D W, et al. 2004. Methane fluxes between terrestrial ecosystems and the atmosphere at northern high latitudes during the past century: A retrospective analysis with a process-based biogeochemistry model. Global Biogeochem Cy, 18: GB3010, doi: 10.1029/2004GB002239

SCIENCE CHINA
Earth Sciences

Appendix 1

Soil hydrothermal parametric formula

The soil heat capacity C ($\mathrm{Jm^{-3}\ K^{-1}}$) (Dai et al., 2007; Oleson et al., 2010) can be calculated as follows:

$$C = C_{\mathrm{g}}\left(1-\theta_{\mathrm{s}}\right)+C_{\mathrm{w}}\theta+C_{\mathrm{i}}\theta_{\mathrm{i}}. \tag{A1}$$

In eq. (A1), θ_{s} is the soil porosity; C_{g}, C_{w}, and C_{i} denote the volumetric heat capacities of soil solids, water, and ice, respectively, and C_{g} can be calculated as:

$$C_{\mathrm{g}} = \left(\frac{2.128(\%\mathrm{sand})+2.385(\%\mathrm{clay})}{\%\mathrm{sand}+\%\mathrm{clay}}\right)\times 10^{6}.$$

$\lambda(z,t)$ is the soil thermal conductivity ($\mathrm{W\ m^{-1}\ K^{-1}}$), denoted as (Dai et al., 2007; Oleson et al., 2010):

$$\lambda = Ke(\lambda_{\mathrm{sat}}-\lambda_{\mathrm{dry}})+\lambda_{\mathrm{dry}}. \tag{A2}$$

In eq. (A2), Ke is the Kersten number, which can be calculated as:

$$Ke = \begin{cases} 0.7\lg S_{\mathrm{r}}+1.0 \geqslant 0, & T \geqslant T_{\mathrm{f}}, \\ S_{\mathrm{r}}, & T < T_{\mathrm{f}}, \end{cases}$$

where $S_{\mathrm{r}} = \dfrac{\theta_{\mathrm{i}}+\theta}{\theta_{\mathrm{s}}} \leqslant 1.$

The thermal conductivities (Dai et al., 2007; Oleson et al., 2010) of saturated soil and dry soil are:

$$\lambda_{\mathrm{sat}} = \lambda_{\mathrm{s}}^{1-\theta_{\mathrm{s}}}\lambda_{\mathrm{i}}^{\theta_{\mathrm{s}}-\theta}\lambda_{\mathrm{l}}^{\theta}, \tag{A3}$$

$$\lambda_{\mathrm{dry}} = \frac{0.135\rho_{\mathrm{d}}+64.7}{2700-0.947\rho_{\mathrm{d}}}, \tag{A4}$$

where $\lambda_{\mathrm{s}}, \lambda_{\mathrm{i}}, \lambda_{\mathrm{l}}$ are the thermal conductivities ($\mathrm{W\ m^{-1}\ K^{-1}}$) of soil solids, ice, and water, respectively; in eq. (A4), ρ_{d} is the bulk density ($\mathrm{kg\ m^{-3}}$) of dry soil, and the thermal conductivity of soil solids λ_{s} (Dai et al., 2007; Oleson et al., 2010) is:

$$\lambda_{\mathrm{s}} = \frac{8.80(\%\mathrm{sand})+2.92(\%\mathrm{clay})}{(\%\mathrm{sand})+(\%\mathrm{clay})}.$$

$D(\theta)$ ($\mathrm{m^2\ s^{-1}}$) and $K(\theta)$ ($\mathrm{m\ s^{-1}}$) are the unsaturated soil hydraulic diffusivity and the unsaturated soil hydraulic conductivity (Dai et al., 2007; Oleson et al., 2010), respectively:

$$D(\theta) = \begin{cases} -\dfrac{\mathrm{b}K_{\mathrm{s}}\psi_{\mathrm{s}}}{\theta_{\mathrm{s}}}\left(\dfrac{\theta}{\theta_{\mathrm{s}}}\right)^{\mathrm{b}+2}, & \text{unfrozen}, \\ -10^{-\theta_{\mathrm{i}}}\dfrac{\mathrm{b}K_{\mathrm{s}}\psi_{\mathrm{s}}}{\theta_{\mathrm{s}}}\left(\dfrac{\theta}{\theta_{\mathrm{s}}}\right)^{\mathrm{b}+2}, & \text{frozen}. \end{cases} \tag{A5}$$

$$K(\theta) = \begin{cases} K_{\mathrm{s}}\left(\dfrac{\theta}{\theta_{\mathrm{s}}}\right)^{2\mathrm{b}+3}, & \text{unfrozen}, \\ -10^{-\theta_{\mathrm{i}}}K_{\mathrm{s}}\left(\dfrac{\theta}{\theta_{\mathrm{s}}}\right)^{2\mathrm{b}+3}, & \text{frozen}, \end{cases} \tag{A6}$$

where K_{s} is the saturated soil hydraulic conductivity ($\mathrm{m\ s^{-1}}$) and ψ_{s} is the saturated water potential.

The phase-change thermal capacity of frozen soil can be set to:

$$C_1 = L_1 \rho_w \frac{d\theta_{max}}{dT}. \tag{A7}$$

Then the equivalent volume heat capacity *Ce*, the equivalent thermal conductivity λe, and the equivalent convection velocity *Ue* of the frozen soil in eq. (2) can be defined as follows (Hu et al., 2006; Shang et al., 2009):

$$Ce = C + C_1, \tag{A8}$$

$$\lambda e = \lambda + D(\theta) C_1, \tag{A9}$$

$$Ue = C_1 \frac{dK(\theta)}{d\theta}. \tag{A10}$$

From eqs. (A8)–(A10), the equivalent specific heat capacity of the frozen soil *Ce* not only contains the specific heat capacity *C*, but also considers the latent heat caused by changes in the soil freezing process. Negative feedback relationships between the soil temperature rising and falling and melting and freezing events are reflected. The equivalent thermal conductivity λe considers not only the soil apparent thermal conductivity λ, but also the latent-heat migration with moisture from the unfrozen zone to the frozen zone (segregation freezing). Thus eq. (2) reflects the physical nature of water and heat-coupled migration in the soil freezing and thawing process. If C_1=*0*, eq. (2) reduces to eq. (1).

A soil water and heat transfer numerical model including changes in soil frost and thaw fronts

For the soil freezing and thawing moving-boundary problems developed in Section 1.1, a local adaptive variable-grid method has been used to discretize the model based on the hierarchical structure of the Community Land Model (CLM). The discrete algorithms for energy balance, soil and water quality equations, and frost and thaw front equations are given as follows.

(1) Discretization of the soil energy equation

Let $\{t_k\}_{k\geqslant 0}$ be a set of time nodes at time *k* with time step Δt. $\Gamma_h = \{z_j; j = 1, 2, \cdots, J\}$ denotes the nodes on interval [0, *L*]. The interfaces s_j are divided into *k*1 and *k*2 FTFs, and their positions are denoted by $\xi_k^{m1}, \varsigma_k^{m2}$, respectively. Set $\Gamma_{h2} = \Gamma_h \bigcup \{\xi_j^1, \cdots, \xi_j^{k1}, \varsigma_j^1, \cdots \varsigma_j^{k2}\}$, $k \geqslant 1$, where Γ_{h2} includes all the grid points of Γ_h plus the interface points. Figure A1 is a schematic diagram with three layers of soil, $j-1, j, j+1$. Soil temperature is defined at each node $z_j (j = 1, 2, \cdots, J_k)$, while the thermal conductivity λ is defined at the interface depth. The thickness of each soil layer $\Delta z_j(m)$ $(j = 1, 2, \cdots, J_k)$ is defined as follows:

$$\Delta z_j = \begin{cases} 0.5(z_1 + z_2), & j = 1, \\ 0.5(z_{j+1} - z_{j-1}), & j = 2, \cdots, J_k - 1, \\ z_j - z_{j-1} & j = J_k. \end{cases}$$

The interface depth $z_{j+\frac{1}{2}}$ (m) is defined as follows:

$$z_{j+\frac{1}{2}} = \begin{cases} 0.5(z_j + z_{j+1}), & j = 1, 2, \cdots J_k - 1, \\ z_j + 0.5\Delta z_j, & j = J_k. \end{cases}$$

The heat flux from the *j*-th to the (*j*+1)st layer, $F_{j+\frac{1}{2}}$ (W m^{-2}), is defined as:

$$F_{j+\frac{1}{2}} = -\lambda_{j+\frac{1}{2}} \frac{T_j - T_{j+1}}{z_{j+1} - z_j}. \tag{A11}$$

In eq. (A11),

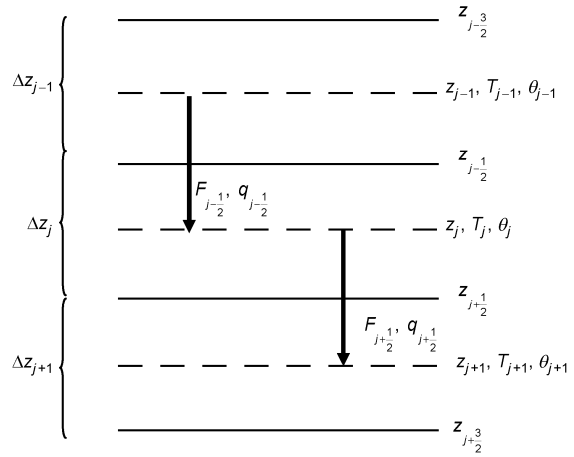

Figure A1 Numerical schematic diagram of soil-water heat flux. z_{j-1}, z_j, z_{j+1} denote node depths, and $z_{j-1/2}$, $z_{j+1/2}$, $z_{j+3/2}$ denote interface depths.

$$\lambda_{j+\frac{1}{2}}=\begin{cases}\dfrac{\lambda_j\lambda_{j+1}(z_{j+1}-z_j)}{\lambda_j\left(z_{j+1}-z_{j+\frac{1}{2}}\right)+\lambda_{j+1}\left(z_{j+\frac{1}{2}}-z_j\right)}, & j=1,\cdots,J_k-1,\\ 0, & j=J_k.\end{cases}$$

Eq. (1) is a special case of eq. (2). Therefore, only the energy portion of eq. (2) is discretized. The full implicit difference discretization formula is as follows:

$$Ce_j^{k+1}\frac{T_j^{k+1}-T_j^k}{\Delta t}=\frac{1}{\Delta z_j}\left[\frac{\lambda e_{j+1/2}^{k+1}\left(T_{j+1}^{k+1}-T_j^{k+1}\right)}{z_{j+1}-z_j}-F_{j-\frac{1}{2}}^{k+1}\right]-Ue_j^{k+1}\frac{T_{j+1}^{k+1}-T_j^{k+1}}{z_{j+1}-z_j},\ j=1; \tag{A12}$$

$$Ce_j^{k+1}\frac{T_j^{k+1}-T_j^k}{\Delta t}=\frac{1}{\Delta z_j}\left[\frac{\lambda e_{j+1/2}^{k+1}\left(T_{j+1}^{k+1}-T_j^{k+1}\right)}{z_{j+1}-z_j}-\frac{\lambda e_{j-1/2}^{k+1}\left(T_j^{k+1}-T_{j-1}^{k+1}\right)}{z_j-z_{j-1}}\right]-Ue_j^{k+1}\frac{T_{j+1}^{k+1}-T_j^{k+1}}{z_{j+1}-z_j}, \tag{A13}$$

$$j=2,\cdots,J_k-1;$$

$$Ce_j^{k+1}\frac{T_j^{k+1}-T_j^k}{\Delta t}=\frac{1}{\Delta z_j}\left[F_{j+\frac{1}{2}}-\frac{\lambda e_{j-1/2}^{k+1}(T_j^{k+1}-T_{j-1}^{k+1})}{z_j-z_{j-1}}\right]-Ue_j^{k+1}\frac{T_j^{k+1}-T_{j-1}^{k+1}}{z_j-z_{j-1}},\quad j=J_k. \tag{A14}$$

Set $E_j=\dfrac{\Delta t}{Ce_j^{k+1}\Delta z_j}$, $j=1,\cdots,J_k$

$a_j=0$, $c_j=-E_j\lambda e_{j+\frac{1}{2}}^{k+1}\dfrac{1}{z_{j+1}-z_j}+\dfrac{\Delta tUe_j^{k+1}}{Ce_j^{k+1}\left(z_{j+1}-z_j\right)}$, $b_j=1-c_j$,

$h_j=T_j^k-E_j\,flux(t)$, $j=1$.

$a_j=-E_j\lambda e_{j-\frac{1}{2}}^{k+1}\dfrac{1}{z_j-z_{j-1}}$, $c_j=-E_j\lambda e_{j+\frac{1}{2}}^{k+1}\dfrac{1}{z_{j+1}-z_j}+\dfrac{\Delta tUe_j^{k+1}}{Ce_j^{k+1}}\dfrac{1}{z_{j+1}-z_j}$ and $b_j=1-a_j-c_j$, $h_j=T_j^k$, $j=2,\cdots,J_k-1$,

$a_j=\left(E_j\lambda e_{j-\frac{1}{2}}^{k+1}\dfrac{1}{z_j-z_{j-1}}+\dfrac{Ue_j^{k+1}\Delta t}{(z_j-z_{j-1})Ce_j^{k+1}}\right)$, $b_j=1-a_j, c_j=0$,

$h_j=T_j^k+E_j\text{Bottomflux}(t)$, $j=J_k$.

Thus, eqs. (A12)–(A14) can be written as:

$$\begin{cases} b_1 T_1^{k+1} + c_1 T_2^{k+1} = h_1, \\ a_j T_{j-1}^{k+1} + b_j T_j^{k+1} + c_j T_{j+1}^{k+1} = h_j,\ j = 2,3,\cdots,J_k - 1, \\ a_{J_k} T_{J_k-1}^{k+1} + b_{J_k} T_{J_k}^{k+1} = h_{J_k}. \end{cases} \tag{A15}$$

(2) Discretization of the vertical one-dimensional unsaturated soil equation

Based on the soil stratification described above, the soil water content is defined at each node $z_j (j = 1,2,\cdots,J_k)$. However, the soil-water hydraulic conductivity $K(\theta)$, the non-saturated soil hydraulic diffusivity $D(\theta)$, and the soil-water flux q are defined at the interface depth. For the soil water flux q, the downward direction is positive (see Figure A1). The full implicit difference discretization formula for soil water in eq. (2) is as follows:

$$\frac{\theta_j^{k+1} - \theta_j^k}{\Delta t} = \frac{D_{j+\frac{1}{2}}^{k+1}\left(\frac{\theta_{j+1}^{k+1} - \theta_j^{k+1}}{z_{j+1} - z_j}\right) - K_{j+\frac{1}{2}}^{k+1} + q_{j-\frac{1}{2}}^{k+1}}{\Delta z_j} - \frac{\rho_{\mathrm{i}}}{\rho_{\mathrm{w}}}\frac{(\theta_{\mathrm{i}})_j^{k+1} - (\theta_{\mathrm{i}})_j^{k+1}}{\Delta \mathrm{t}},\ j = 1, \tag{A16}$$

$$\frac{\theta_j^{k+1} - \theta_j^k}{\Delta t} = \frac{D_{j+\frac{1}{2}}^{k+1}\left(\frac{\theta_{j+1}^{k+1} - \theta_j^{k+1}}{z_{j+1} - z_j}\right) - D_{j-\frac{1}{2}}^{k+1}\left(\frac{\theta_j^{k+1} - \theta_{j-1}^{k+1}}{z_j - z_{j-1}}\right)}{\Delta z_j} - \frac{K_{j+\frac{1}{2}}^{k+1} - K_{j-\frac{1}{2}}^{k+1}}{\Delta z_j} - \frac{\rho_{\mathrm{i}}}{\rho_{\mathrm{w}}}\frac{(\theta_{\mathrm{i}})_j^{k+1} - (\theta_{\mathrm{i}})_j^{k+1}}{\Delta \mathrm{t}},\ j = 2,3,\cdots,J_k - 1, \tag{A17}$$

$$\frac{\theta_j^{k+1} - \theta_j^k}{\Delta t} = \frac{0 - D_{j-\frac{1}{2}}^{k+1}\left(\frac{\theta_j^{k+1} - \theta_{j-1}^{k+1}}{z_j - z_{j-1}}\right) + K_{j-\frac{1}{2}}^{k+1}}{\Delta z_j} - \frac{\rho_{\mathrm{i}}}{\rho_{\mathrm{w}}}\frac{(\theta_{\mathrm{i}})_j^{k+1} - (\theta_{\mathrm{i}})_j^{k+1}}{\Delta \mathrm{t}},\ j = J_k. \tag{A18}$$

Set

$$\alpha_1 = 0,\ \beta_1 = 1 + \frac{\Delta t D_{\frac{3}{2}}^{k+1}}{\Delta z_1 (z_2 - z_1)},\ \gamma_1 = -\frac{\Delta t D_{\frac{3}{2}}^{k+1}}{\Delta z_1 (z_2 - z_1)},\ \delta_1 = \theta_1 - \frac{\Delta t}{\Delta z_1}\left(K_{\frac{3}{2}}^{k+1} - q_{\frac{1}{2}}^{k+1}\right) - \frac{\rho_{\mathrm{i}}}{\rho_{\mathrm{w}}}\frac{(\theta_{\mathrm{i}})_j^{k+1} - (\theta_{\mathrm{i}})_j^{k+1}}{\Delta \mathrm{t}};$$

$$\alpha_j = -\frac{\Delta t D_{j-\frac{1}{2}}^{k+1}}{\Delta z_j (z_j - z_{j-1})},\ \beta_j = 1 + \frac{\Delta t D_{j+\frac{1}{2}}^{k+1}}{\Delta z_j (z_{j+1} - z_j)} + \frac{\Delta t D_{j-\frac{1}{2}}^{k+1}}{\Delta z_j (z_j - z_{j-1})},\ \gamma_j = -\frac{\Delta t D_{j+\frac{1}{2}}^{k+1}}{\Delta z_j (z_{j+1} - z_j)},$$

$$\delta_j = \theta_j^k - \frac{\Delta t}{\Delta z_j}\left(K_{j+\frac{1}{2}}^{k+1} - K_{j-\frac{1}{2}}^{k+1}\right) - \frac{\rho_{\mathrm{i}}}{\rho_{\mathrm{w}}}\frac{(\theta_{\mathrm{i}})_j^{k+1} - (\theta_{\mathrm{i}})_j^{k+1}}{\Delta \mathrm{t}},\ j = 2,3,\cdots,J_k - 1;$$

$$\alpha_{J_k} = -\frac{\Delta t D_{J_k-\frac{1}{2}}^{k+1}}{\Delta z_{J_k}(z_{J_k} - z_{J_k-1})},\ \beta_{J_k} = 1 + \frac{\Delta t D_{J_k-\frac{1}{2}}^{k+1}}{\Delta z_{J_k}(z_{J_k} - z_{J_k-1})},\ \gamma_{J_k} = 0,$$

$$\delta_{J_k} = \theta_{J_k}^k + \frac{\Delta t}{\Delta z_{J_k}} K_{J_k-\frac{1}{2}}^{k+1} - \frac{\rho_{\mathrm{i}}}{\rho_{\mathrm{w}}}\frac{(\theta_{\mathrm{i}})_j^{k+1} - (\theta_{\mathrm{i}})_j^{k+1}}{\Delta \mathrm{t}}.$$

Therefore, eqs. (A16)–(A18) can be written as follows:

$$\begin{cases} \beta_1\theta_1^{k+1} + \gamma_1\theta_2^{k+1} = \delta_1, \\ \alpha_j\theta_{j-1}^{k+1} + \beta_j\theta_j^{k+1} + \gamma_j\theta_{j+1}^{k+1} = \delta_j, \quad j = 2,3,\cdots,J_k - 1. \\ \alpha_{J_k}\theta_{J_k-1}^{k+1} + \beta_{J_k}\theta_{J_k}^{k+1} = \delta_{J_k}, \end{cases} \tag{A19}$$

(3) Discretization of the frost and thaw front equations

Assume that the temperature of the soil layer changes continuously. Let position $s_j(t_k)$ of the j-th FTF depth at time t_k be denoted as s_j^k. The position s_j^k in the hierarchical soil structure is shown in Figure (A2). The moving-interface eq. (4) can be discretized as follows:

$$\pm Q^{k+1}\left(\frac{s_j^{k+1} - s_j^k}{\Delta t}\right) = \lambda_{j1+1/2}^{k+1}\frac{T_{j1}^{k+1} - T_{\mathrm{f}}}{s_j^k - z_{j1}} - \lambda_{j1+3/2}^{k+1}\frac{T_{\mathrm{f}} - T_{j1}^{k+1}}{z_{j1+2} - s_j^k}. \tag{A20}$$

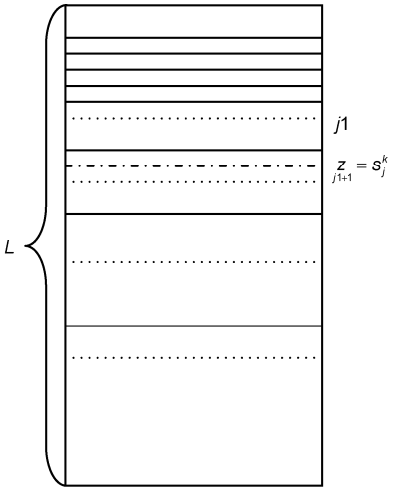

Figure A2 Adaptive grid for simulating FTF.